Available online at www.sciencedirect.com
SCIENCE DIRECT®
Inorganica Chimica Acta 357 (2004) 1931–1947
Inorganica Chimica Acta
www.elsevier.com/locate/ica

Strain in organometallics II: controlling the properties of tetra-coordinated iridium complexes using diastereomers of a bis(tropp) ligand system ☆

Cècile Laporte, Torsten Büttner, Heinz Rüegger, Jens Geier, Hartmut Schönberg, Hansjörg Grützmacher *

Department of Chemistry and Applied Biosciences, ETH-Hönggerberg, Zürich CH-8093, Switzerland

Received 26 November 2003; accepted 21 January 2004

Dedicated to Prof. Helmut Werner on the occasion of his 70th birthday

Abstract

The tetra-chelating ligands 1,2-bis[(5H-dibenzo[*a*,*d*]cyclohepten-5-yl)phenylphosphanyl]-ethane, bis(tropp^{Ph})ethane, and 1,3-bis[(5H-dibenzo[*a*,*d*]cyclohepten-5-yl)phenylphosphanyl]-propane, bis(tropp^{Ph})propane, were synthesised. For the binding of transition metals, these ligands offer two olefin moieties and two phosphorus centres and form mixtures of diastereomers with a *R*,*S*-configuration at the phosphorus centres (*meso*), or a *R*,*R*(*S*,*S*)-configuration (*rac*), respectively. *meso*/*rac*-bis(tropp^{Ph})ethane was separated by fractional crystallisation and reacted with [Ir(cod)$_2$]OTf (cod = cylcooctadiene, OTf$^-$ = $CF_3SO_3^-$) to give the penta-coordinated complex-cations *meso*/*rac*-[Ir(bis(tropp^{Ph})ethane)(cod)]$^+$, where the bis(tropp^{Ph})ethane serves as tridentate ligand merely. One olefin unit remains non-bonded, however, a slow intra-molecular exchange between this olefin and the coordinated olefin unit was established (*meso*-[Ir(bis(tropp^{Ph})ethane)(cod)]$^+$: $k < 0.5$ s^{-1}; *rac*-[Ir(bis(tropp^{Ph})ethane)(cod)]$^+$: $k \approx 35$ s^{-1}). The ligand *meso*/*rac*-bis(tropp^{Ph})propane reacts with [Ir(cod)$_2$]OTf to give the corresponding complexes containing the tetra-coordinated 16-electron complex-cations *meso*/*rac*-[Ir(bis(tropp^{Ph})propane)]$^+$. The diastereomers were separated by fractional crystallisation. The complex *rac*-[Ir(bis(tropp^{Ph})propane)]$^+$ is reduced at relatively low potentials ($E^1_{1/2} = -0.95$ V, $E^2_{1/2} = -1.33$ V versus Ag/AgCl) to give the neutral 17-electron complex [Ir(bis(tropp^{Ph})propane)]^0 and the 18-electron anionic iridate [Ir(bis(tropp^{Ph})propane)]$^-$, respectively. With acetonitrile, [Ir(bis(tropp^{Ph})propane)]$^+$ reacts to give the penta-coordinated complex *rac*-[Ir(MeCN)(bis(tropp^{Ph})propane)]$^+$ ($K = 45$ M^{-1}, $k_f = 6 \times 10^3$ M^{-1} s^{-1}, $k_d = 1 \times 10^2$ s^{-1}) and with chloride to yield the relatively stable complex *rac*-[Ir(Cl)(bis(tropp^{Ph})propane)] ($k_d < 0.5$ s^{-1}). Compared to the *rac*-isomer, the *meso*-[Ir(bis(tropp^{Ph})propane)]$^+$ shows significantly cathodically shifted reduction potentials ($E^1_{1/2} = -1.25$ V, $E^2_{1/2} = -1.64$ V versus Ag/AgCl), an acetonitrile complex could not be detected, and the chloro-complex, *meso*-[Ir(Cl)(bis(tropp^{Ph})propane)], is much more labile ($k_d \approx 20'000$ s^{-1}). *meso*-[Ir(bis(tropp^{Ph})propane)]$^+$ reacts with one equivalent H_2 to give the *trans*-dihydride complex-cation, *meso*-[Ir(H)$_2$(bis(tropp^{Ph})propane)]$^+$, while the *rac*-isomer, *rac*-[Ir(bis(tropp^{Ph})propane)]+, reacts with two equivalents H_2 to give *rac*-{Ir(H)$_2$(OTf)[(tropp^{Ph})(H$_2$tropp^{Ph})propane]}, a *cis*-dihydride complex containing a hydrogenated 10,11-dihydro-5H-dibenzo[*a*,*d*]cycloheptene unit, H$_2$tropp^{Ph}. The triflate anion in this complex is rather firmly bound and dissociates only slowly ($k = 29$ s^{-1}). All differences between the different stereoisomers are attributed to the fact that the ligand backbone in the *meso*-isomer, *meso*-[Ir(bis(tropp^{Ph})propane)]$^+$, enforces a planar coordination sphere at the metal. On the contrary, already in the tetra-coordinated *rac*-[Ir(bis(tropp^{Ph})propane)]$^+$, the metal has a tetrahedrally distorted coordination sphere which does not impede the reduction to the d^9-Ir(0) and d^{10}-Ir(−1) complexes and allows more easily a distortion towards a trigonal bipyramidal (tbp) or octahedral structure for penta- or hexa-coordinated complexes, respectively. A comparison of the NMR data for iridium bonded

☆ Supplementary data associated with this article can be found, in the online version, at doi:10.1016/j.ica.2004.01.034.

* Corresponding author. Present address: Department of Chemistry and Applied Biosciences, HCI, ETH-Hönggerberg, Zürich CH-8093, Switzerland. Tel.: +004116322855; fax: +004116331032.

E-mail address: gruetzmacher@inorg.chem.ethz.ch (H. Grützmacher).

0020-1693/$ - see front matter © 2004 Published by Elsevier B.V.
doi:10.1016/j.ica.2004.01.034

olefins in equatorial or axial positions in tbp structures shows that the latter experience only modest metal-to-ligand back-donation, while the olefins in the equatorial positions have a high degree of metallacyclopropane character.

Keywords: Hydrogenation; Iridium; Kinetic data; Mechanism; Redox chemistry; Stereochemistry; Structure reactivity relationships

1. Introduction

To influence the reactivity of transition metal complexes by enforcing particular conformations is a widely used approach in organometallic chemistry. Classical examples include the stabilisation of complexes $[ML_2X_2]$ against loss of X_2 in a reductive elimination by imposing a *trans*-configuration or, inversely, activating a $[ML_2]$ fragment for oxidative addition by fixing a *cis*-configuration and a small L–M–L angle [1]. "Strain energy" had a profound impact on the properties of an organometallic in the following examples: (i) The influence of ring strain in $M(R_2P\cap PR_2)$ heterocycles on the activation barrier, $\Delta G^{\#}$, for Berry-rotation in trigonal bipyramidal $[M(CH_3)(R_2P\cap PR_2)(cod)]$ complexes with $\cap = (CH_2)_n$; $n = 2, 3$ [2]. It was found that complexes with chelating bis(phosphanes) have lower $\Delta G^{\#}$'s than $[M(CH_3)(PR_3)_2(cod)]$ with two monodentate PR_3 ligands, and that the smaller chelate ring $R_2P–(CH_2)_2–PR_2$ favours faster isomerisation than the larger chelate $R_2P–(CH_2)_3–PR_2$. (ii) The concept of the *natural bite angle* and *flexibility range* was introduced by Casey and Whiteker [3] in order to predict the structures and reactivity of metal complexes with chelating ligands (based on molecular mechanics calculations). Following early theoretical work [4] indicating that ligands with a large bite angle will facilitate migratory insertion steps in catalytic cycles, this concept was recently successfully exploited especially by van Leeuwen and coworkers [5]. In various catalytic reactions (hydroformylation, allylic substitutions, aminations, hydrocyanations), *wide bite angle* bis(phosphanes) proved to be superior ligands giving higher activities and selectivities. Further examples concern the polymerisation of olefins with strained *ansa*-ferrocenes [6], inter-molecular C–H and C–C activation with *ansa*-molybdenocenes [7], or the preparation of organometallic plastics in ring opening polymerisation processes using strained cyclic *ansa*-ferrocenes as monomers. In the latter case, Manners [8] determined the strain energies of such compounds by calorimetric methods to be in the order of 60–90 kJ/mol.

In previous work, we described tropp type phosphanes **I** (*trop*ylidenyl *p*hosphane; IUPAC = 5-diphenylphosphanyl-5H-dibenzo[*a*,*d*]cycloheptene) [9] as suitable ligand system for the preparation of mono-nuclear para-magnetic 17-electron rhodium(0) [10,11] and iridium(0) complexes by reduction of complexes like *trans*/*cis*-**II** (Scheme 1) [12]. Further stable and isolated compounds of this type have been reported but are still very rare [13,14].

We became interested in the problem of creating strained organometallic molecules as one possibility of controlling their redox potentials. This concept has been impressively applied for complexes with metals of the 4th period, i.e., for Ni(II)/Ni(I) [15] and Cu(II)/Cu(I), [16] and is of fundamental importance for the understanding of structure–reactivity-relationships and the design of redox chains. Tetra-coordinated Ni(II) and Cu(II) complexes prefer planar or square pyramidal ground state structures, while the reduced species, i.e., Ni(I) and Cu(I), favour tetrahedral forms. By enforcing a tetrahedral structure, the redox potentials could be raised substantially (i.e., shifted anodically). With this perspective, Longato et al. [13a] and we [17] prepared strongly tetrahedrally distorted 16-electron rhodium(I) complexes, $[Rh(dppf)_2]^+$ and $[Rh(^{Me}tropp^{Ph})_2]^+$ with dppf = 1,1′-bis(diphenylphosphanyl)ferrocene and $^{Me}tropp^{Ph}$ = 5-diphenylphosphanyl-10-methyl-5H-dibenzo[*a*,*d*]cycloheptene, respectively, but failed to observe any significant effect on the redox potentials. We then turned our attention to an alternative approach which consists in confining the structure of the reduced 17-electron rhodium(0) complex to a square planar one. Since these compounds prefer tetrahedral structures, a significant cathodic shift of the redox potential was expected.

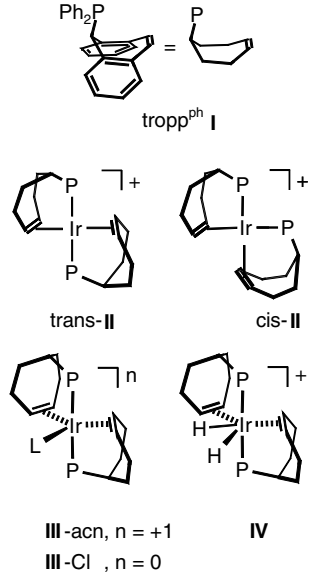

Scheme 1. Depiction of the 5-diphenylphosphanyl-5H-dibenzo[*a*,*d*]cycloheptene, $tropp^{Ph\ I}$, the 16-electron iridium(I) complexes *trans*-**II** and *cis*-**II**, the 18-electron iridium(I) complexes **III**-acn, **III**-Cl, and the *cis*-dihydride **IV**.

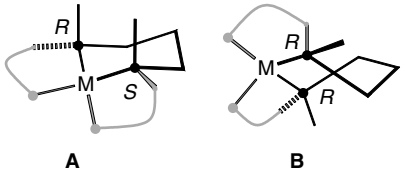

Scheme 2. Schematic representation of a tetra-dentate ligand with a central six-membered chelate ring. For the *R*,*S*-stereochemistry, a planar for a *R*,*R*(*S*,*S*)-stereochemistry, a tetrahedrally distorted coordination sphere at a tetracoordinated d^8-metal centre is expected.

Based on simple Dreiding-models, it occurred to us that the investigation of especially designed tetra-chelating ligands which give rise to two diastereomers may be interesting in this respect. A sketch is given in Scheme 2 for an achiral *R*,*S*-configured ligand and a chiral *R*,*R*(*S*,*S*)-configured ligand. A d^8 metal M that prefers a square planar coordination sphere gives with the *R*,*S*-configured ligand a complex **A** where the bulky gray-shaded arms of the chelate occupy the equatorial sites of the central six-membered ring (shown in black). This conformation should be quite rigid and impede distortions to a tetrahedral form. With the *R*,*R*(*S*,*S*)-isomer, a tetrahedrally distorted coordination sphere at the metal together with a twist-like conformation of the central chelate ring should be the best compromise to minimise unfavourable electronic and steric interactions.

We found that in a complex of type **A** with $M = d^8$-Rh, the reduction to a d^9-rhodium(0) complex occurred at significantly more negative potentials which indicated that our concept of controlling the redox potential of such complexes might be correct [18]. In this paper, we give a full account of our work concerning the investigation of comparable iridium complexes with tetrachelating bis(tropp) ligand systems which, in particular, allowed the synthesis and separation of both diastereomers of type **A** and **B** and a much better validation of our concept.

2. Syntheses of ligands

The ligand syntheses are out-lined in Scheme 3 and start with 1,2-bis-(phenylphosphanyl)ethane **1** or 1,3-bis-(phenylphosphanyl)propane **2**, respectively, which are converted to the corresponding secondary bis(phosphanes) **3** and **4** following a method described in the literature [19].

As discussed in part in a previous paper [18], the bis(phosphanes) **3** and **4** react with 5-chloro-5H-dibenzo[*a*,*d*]cycloheptene **5** (tropCl) to give the desired chelating phosphanes as a mixture of *R*,*S*-**6, 7**, and the racemates *R*,*R*- and *S*,*S*-**6, 7** in about 60–70% yield. We will refer to the *R*,*S*-configured diastereomers as *meso*-bis(tropp^{Ph})ethane, *meso*-**6**, and *meso*-bis(tropp^{Ph})propane, *meso*-**7**, and to the chiral *R*,*R*(*S*,*S*)-forms as

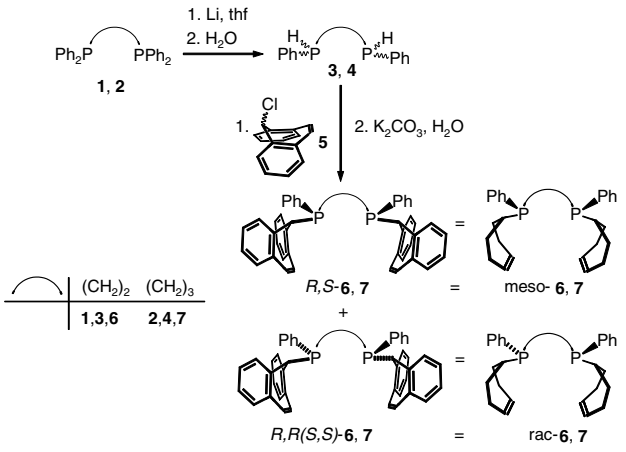

Scheme 3. Syntheses of bis(tropp^{Ph})ethane *R*,*S*-**6** (*meso*-**6**), *R*,*R*(*S*,*S*)-**6** (*rac*-**6**) and bis(tropp^{Ph})propane *R*,*S*-**7** (*meso*-**7**), *R*,*R*(*S*,*S*)-**7** (*rac*-**7**).

rac-bis(tropp^{Ph})ethane, *rac*-**6**, and *rac*-bis(tropp^{Ph})propane, *rac*-**7**, in the following. While the diastereomers of the ethyl-bridged derivative **6** could be separated by fractional crystallisation, all attempts to separate the isomers of the propylene-bridged compound **7** failed. However, the diastereomers of the bis(tropp^{Ph})propane (and its cationic square planar complexes, vide infra) can be easily distinguished on the basis of their ^{1}H NMR spectra. For symmetry reasons, one expects the C_s symmetric *meso*-**7** to show *four* different resonances while the C_2 symmetric *rac*-**7** should show only *three* different signals for the methylene protons in the $(CH_2)_3$-bridge (see Fig. 2 for an illustration).

The following assignments were made in the expanded region of the ^{1}H NMR spectrum (shown in Fig. 2) for the CH_2 resonances (based on ^{31}P–^{1}H and ^{13}C–^{1}H correlation experiments): The broad signal at 0.86 ppm is due to a superposition of the H_3 and H_4 resonances of the meso compound. The signal at 0.97 ppm is assigned to H_3 of the racemic compound due to its multiplicity and integrated intensity. By means of a ^{31}P, ^{1}H correlation, it is then possible to assign all other proton signals, as well as the phosphorus resonances, to distinct diastereomers.

3. Syntheses of complexes

The ligands bis(tropp^{Ph})ethane **6** and bis(tropp^{Ph})propane **7** were reacted with the complex [Ir(cod)$_2$]Otf **8** ($OTf^- = CF_3SO_3^-$) as iridium-source in methylene chloride as solvent. The separated diastereomers, *meso*-**6** and *rac*-**6**, were reacted to give the complexes *meso*-**9** and *rac*-**9** (Scheme 4) which were isolated as pale-yellow powders after addition of *n*-hexane to the reaction medium. With **7**, the mixture of diastereomers was reacted with **8** in CH_2Cl_2 and the complexes *meso*-**10** and *rac*-**10** were obtained with 82% yield as micro-crystalline dark-red

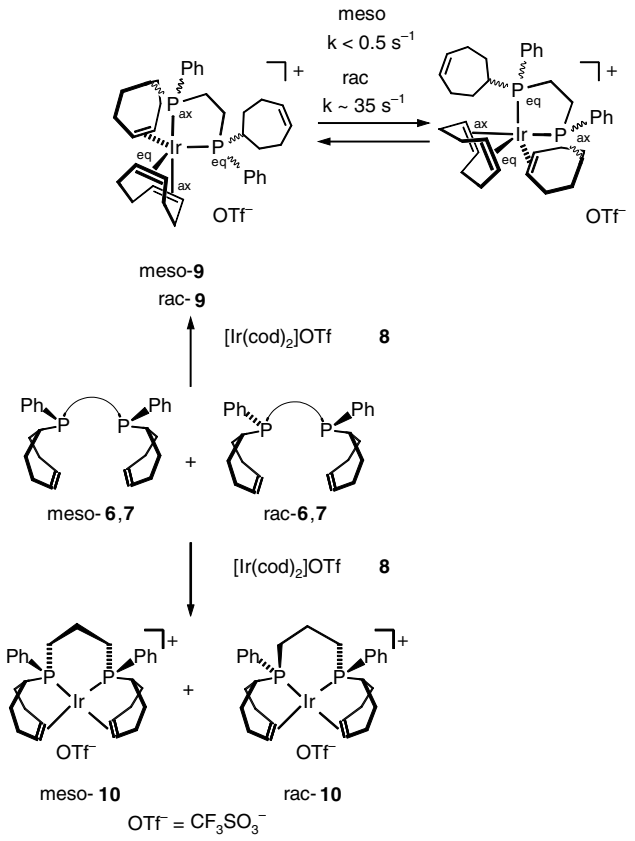

Scheme 4. Synthesis of the iridium(I) complexes *meso*/*rac*-**9** and *meso*/*rac*-**10** and molecular dynamics encountered in *meso*/*rac*-**9**.

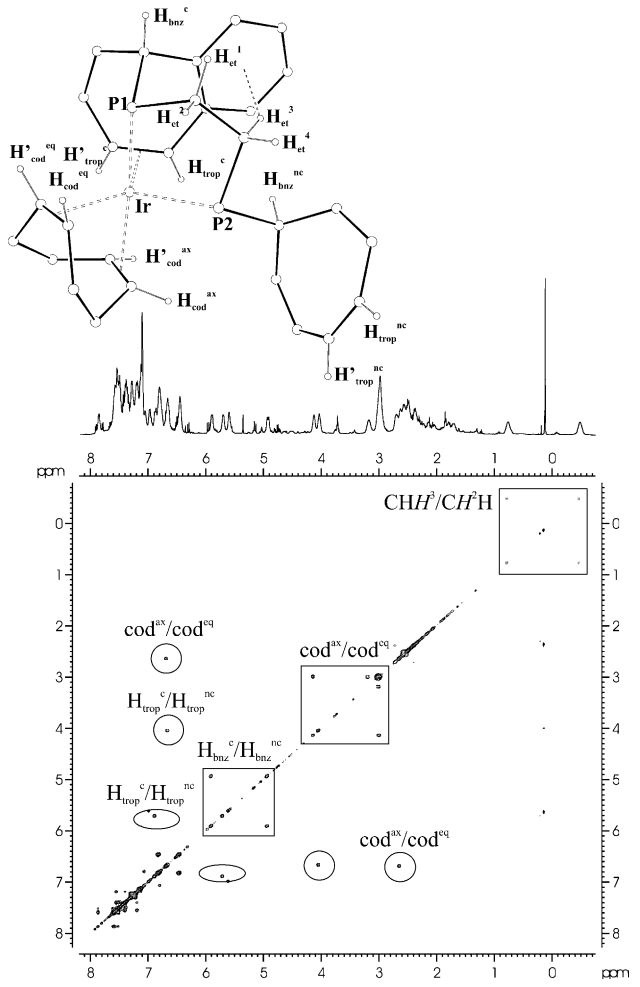

Fig. 1. ^{1}H NOESY spectrum of *rac*-**9** at $T = 298$ K. The molecular graph, which is used to assign the resonances, is based on the structure of *meso*-**9** which was determined by X-ray analysis [17].

powder after precipitation with *n*-hexane from the reaction medium (Scheme 4). By fractional crystallisation from thf, *meso*-**10** and *rac*-**10** could be separated and *rac*-**10** was obtained in pure form. The *meso*-isomer was always contaminated with residual *rac*-**10** (about 10%) but could be characterised by NMR spectroscopy.

The synthesis and structure of *meso*-**9** as penta-coordinated iridium complex with the bis(tropp^{Ph})ethane **6** acting merely as a tridentate ligand, which displaces only one cod ligand from **8**, was previously reported [18]. The structure of *rac*-**9** could not be determined by X-ray analysis. In the ^{31}P NMR spectrum, the complex *meso*-**9** shows two sharp signals at 12.7 ppm (P2) and 66.6 ppm (P1) while the corresponding resonances at 39.1 ppm (P2) and 77.6 ppm (P1) for *rac*-**9** are broad and indicate an exchange phenomenon (see Fig. 1 for assignments). The ^{1}H and ^{13}C NMR spectra of both *meso*-**9** and *rac*-**9** are rather complex and difficult to interpret fully, especially for *rac*-**9** because of additional exchange broadening (see Fig. 1).

However, at −60 °C a sufficiently well-resolved ^{1}H spectrum was obtained and the most characteristic proton resonances in *rac*-**9** could be assigned. A simplified sketch of the structures with P1 and one C=C$_{cod}$ bond in the axial and P2, the coordinated C=C$_{trop}$ unit, and the second C=C$_{cod}$ bond in the equatorial positions of a trigonal bipyramid is given in Fig. 1 together with the ^{1}H NOESY spectrum of *rac*-**9** at room temperature. Some of the relevant ^{1}H NMR data of *rac*-**9** are listed in Table 1.

Noteworthy, the axially bonded olefinic protons of the cod ligand, H^{ax}_{cod}, H'^{ax}_{cod}, at significantly higher frequency than the protons in equatorial position, H^{eq}_{cod}, H'^{eq}_{cod}, indicate that back-bonding is much less effective for the axially bonded olefin unit [20]. In the structure of *meso*-**9**, this is reflected in the longer Ir–olefin (2.22 Å to the centroid of the C=C bond) and shorter C=C bond of the axial (1.38 Å) compared to the shorter Ir–olefin (2.07 Å) and longer C=C bond (1.41 Å) of the equatorially positioned olefin unit. Furthermore, a strongly shielded resonance at −0.26 ppm in *meso*-**9** and −0.69 ppm in *rac*-**9** is observed for one of the four inequivalent protons in the ethylene-bridge. Inspection of the structure of *meso*-**9** indicates that this signal stems very likely from H^3_{et} with a distance of about 2.8 Å to the midpoint of one of the benzene rings of the coordinated tropp ligands (see structure sketch in Fig. 1). This observation

Table 1
Selected NMR data for *meso*-**9** and *rac*-**9**

	Coordinated trop $\delta(^1H^c)$	Non-coordinated trop $\delta(^1H^{nc})$	Cod (equatorial) $\delta(^1H^{eq})$	Cod (axial) $\delta(^1H^{ax})$
H_{bnz}	4.92	5.84	–	–
H_{olefin}	3.94, $^2J(P,H) = 7.7$ Hz	6.64	2.53	4.05
H'_{olefin}	5.60, $^2J(P,H) = 9.7$ Hz	6.85	2.88	6.64

Chemical shifts in ppm (vs. tms).

also indicates that the structures of *meso*-**9** and *rac*-**9** are rather similar and differ only in the stereochemistry at the equatorially bonded P2-atom.

The dynamic phenomenon in *rac*-**9**, leading to the broad NMR signals at room temperature was elucidated by means of a ^1H NOESY experiment (Fig. 1). Cross-peaks for the axially and equatorially bonded C═C_{cod} protons (H^{ax}_{cod}, H'^{ax}_{cod}/H^{eq}_{cod}, H'^{eq}_{cod}) indicate their mutual exchange. Furthermore, cross-peaks between (i) the olefinic protons of the coordinated (H^{c}_{trop}, H'^{c}_{trop}) and non-coordinated (H^{nc}_{trop}, H'^{nc}_{trop}) tropp ligand, (ii) the benzylic proton of the coordinated (H^{c}_{bnz}) and the non-coordinated one (H^{nc}_{bnz}), and (iii), the ethylene-bridge protons H^3_{et} and H^2_{et} are observed. One possibility to explain the exchange of the cod olefin protons is to assume a simple rotation of the cod ligand. The exchange of the olefinic and benzylic protons of the coordinated and non-coordinated trop ligand as well as the exchange of the protons in the ethylene bridge is explained by an intra-molecular substitution reaction. If the cod ligand did not rotate, this substitution would have to proceed with an accompanying exchange of the axial and equatorial cod protons.

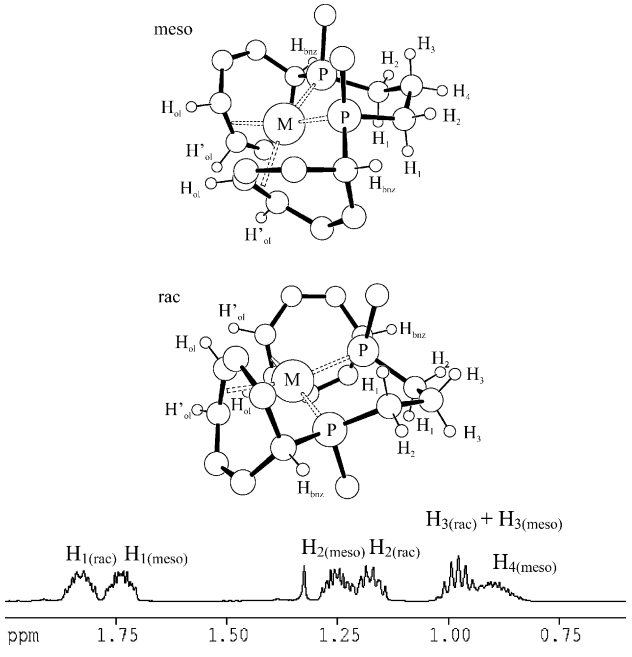

Fig. 2. Sketches of the [M(bis(tropp^{Ph})propane)]$^+$ cations (M = Rh, Ir). The benzo-groups of the tropp ligand and the P-bonded phenyl groups are not shown. Only the *ipso*-carbon atom attached to phosphorus is depicted. The denomination of symmetry equivalent protons in the propylene bridge is indicated. On the bottom, the expanded region of the CH_2-resonances in the ^1H NMR spectrum of a mixture of *meso*/*rac*-**7** is shown.

In that case, the intramolecular substitution resembles a Berry-rotation in the sense that the axial and equatorial phosphorus atoms and the axial and equatorial cod olefin protons interchange. However, in view of the steric encumbrance of the complexes it is more likely that the substitution proceeds via a tetra-coordinated intermediate with only the two phosphorus atoms P1 and P2 and the cod ligand coordinated to iridium while both C═C_{trop} units are non-bonding. In such a mechanism the tetra-coordinated intermediate obtained from *meso*-**9** would have both bulky trop units on the same side of the five-membered chelate ring which should be unfavourable and diminish the intra-molecular exchange rate. An estimation from a line shape analysis of the ^{31}P resonances indicates that this process proceeds with $k \approx 35$ s^{-1} for *rac*-**9**, while for *meso*-**9** this process is too slow ($k < 0.5$ s^{-1}) to be measured by this technique.

The structures of the iridum complexes *meso*-**10** and *rac*-**10** with the bis(tropp^{Ph})propane ligand **7** were not determined by X-ray analyses. However, the structures of the analogous rhodium complexes are known [21] and sketches of these are shown in Fig. 2. The similarity of the NMR data leave no doubt that the iridium complexes have very similar structures, i.e., the central six-membered chelate ring has the expected chair con-

Table 2
Selected NMR data for *meso*-**10** and *rac*-**10**

	δ ^1H and ^{13}C, *meso*-**10**	δ ^1H and ^{13}C, *rac*-**10**
H_{bnz}	5.04 [m, $^2J(P,H) + {}^4J(P,H) = 14.2$ Hz]	5.56 [m, $^2J(P,H) + {}^4J(P,H) = 14.6$ Hz]
H_{ol}	5.74 [d, $^3J(H,H) = 9.4$ Hz]	5.27 [dd, $^3J(H,H) = 9.4$ Hz, $^3J(P,H) = 2.4$ Hz]
H'_{ol}	6.02 [dd, $^3J(H,H) = 9.4$ Hz, $^3J(P,H) = 2.1$ Hz]	6.65 (m)
C_{ol}	85.0 [m, $^2J(P,C) + {}^2J(P',C) = 10.4$ Hz]	79.7 [m, $^2J(P,C) + {}^2J(P',C) = 13.1$ Hz]
C'_{ol}	91.8 [m, $^2J(P,C) + {}^2J(P',C) = 8.4$ Hz]	93.2 [m, $^2J(P,C) + {}^2J(P',C) = 5.1$ Hz]

Chemical shifts in ppm (vs. tms).

formation, while in the other diastereomer a twist conformation is observed. As a consequence, the coordination sphere around the metal centre in the racemic *R*,*R*(*S*,*S*)-configured isomers deviates significantly stronger from the electronically preferred planarity than in the meso form. In *rac*-**10** this is manifested in a rather large difference between the ^{1}H chemical shifts of the two inequivalent protons H_{ol} and H'_{ol} ($\Delta\delta = 1.38$), which is much smaller in *meso*-**10** ($\Delta\delta = 0.28$). As frequently observed for iridium complexes, the ^{1}H and ^{13}C NMR signals of the coordinated tropp-olefin units in *meso*-**10** and *rac*-**10** (Table 2) are shifted to lower frequencies when compared to the rhodium analogues indicating a higher degree of back-bonding.

The characteristic patterns for the CH_2 protons in the propylene bridge, as in the diastereomers of the free ligand *meso*/*rac*-**7**, are observed (bottom of Fig. 2) and prove that C_s- and C_2-symmetric complexes were obtained, respectively, in which the bis(tropp^{Ph})propane acts as tetra-dentate ligand.

4. Reactivity studies

4.1. Redox chemistry

The reduction of the tetra-coordinated 16-electron iridium complexes *meso*-**10** and *rac*-**10** was investigated by cyclic voltammetry (Scheme 5). With sodium naphthalenide as reducing agent, the 18-electron iridate complex *rac*-**12** was synthezised and isolated. A solution of a mixture of *meso*/*rac*-**10** in thf shows three quasi-reversible redox waves in a 1:2:1 intensity ratio. The central wave is the result of a superposition of the second redox wave of one diastereomer with the first redox wave of the other. Pure *rac*-**10** shows two quasi-reversible waves (see Fig. 3), which correspond with the first two waves in the cyclic voltammogram of the mixture. Hence, the both waves at more negative potentials are attributed to *meso*-**10**. The redox potentials versus Ag/AgCl, obtained in thf with 1 M $(n\mathrm{Bu_4N})^+PF_6^-$ as electrolyte at a scan rate of 100 mV/s, are listed in Table 3. In addition, the potential for the iridium complex **II** (see Scheme 1) with the bidentate tropp ligand tropp^{Ph} [12] is given.

The difference of the redox potentials, ΔE, measures the thermodynamic difference between redox couples. Clearly, *meso*-**10** has a more negative reduction potential than *rac*-**10**, i.e., the relative thermodynamic difference between the 16-electron complex *meso*-**10** and 17-electron complex *meso*-**11** is significantly larger. Note that *rac*-**10** has a redox potential very similar to [Ir(tropp^{Ph})$_2$]Otf **II**. A straightforward explanation for the cathodically shifted potential for *meso*-**10** is that the ligand *meso*-**7** cannot adapt to the electronically preferred tetrahedral form of the 17-electron species, which consequently is destabilised. For the other complexes,

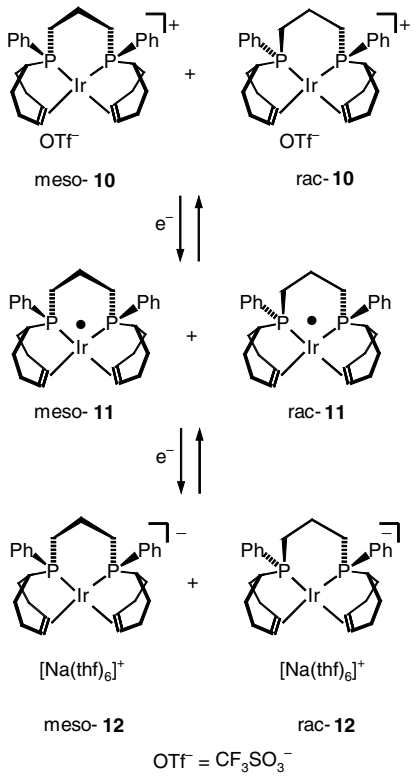

Scheme 5. Reduction of the 16-electron complexes *meso*-**10** and *rac*-**10** to give the 17-electron complexes *meso*-**11** and *rac*-**11** and 18-electron iridate complexes *meso*-**12** and *rac*-**12**.

rac-**10** and **II**, a distortion towards a more tetrahedral structure is easily possible. The significant shift of the redox potentials to more negative values by at least 200 mV indicates that approximately 20 kJ mol^{-1} of strain energy is built up when the compound *meso*-**10** is reduced.

4.2. Reaction with acetonitrile

When an excess of acetonitrile is added to a deeply coloured CH_2Cl_2 solution of a mixture of the tetra-coordinated 16-electron complexes [Ir(bis(tropp^{Ph})propane)]$^+$ Otf$^-$, *meso*-**10** and *rac*-**10**, an immediate colour change occurs.

A ^{31}P NMR spectrum of the reaction mixture at room temperature shows the unaffected resonance of *meso*-**10** and two new broad signals at 20.1 and 27.8 ppm. Lowering the temperature leads to sharpening of these resonances which eventually become two doublets [$^2J(P,P) = 22.1$ Hz]. Only the *rac*-**10** isomer reacts with acetonitrile to give a penta-coordinated complex *rac*-**13** while the *meso*-isomer is inert (Scheme 6). It is possible to isolate *rac*-**13** as yellow precipitate when n-hexane is added to the reaction mixture obtained with pure *rac*-**10** in CH_2Cl_2/ acetonitrile. However, the coordinated acetonitrile ligand is easily lost under quantitative formation of *rac*-**10**. The penta-coordinated complex *rac*-**13**

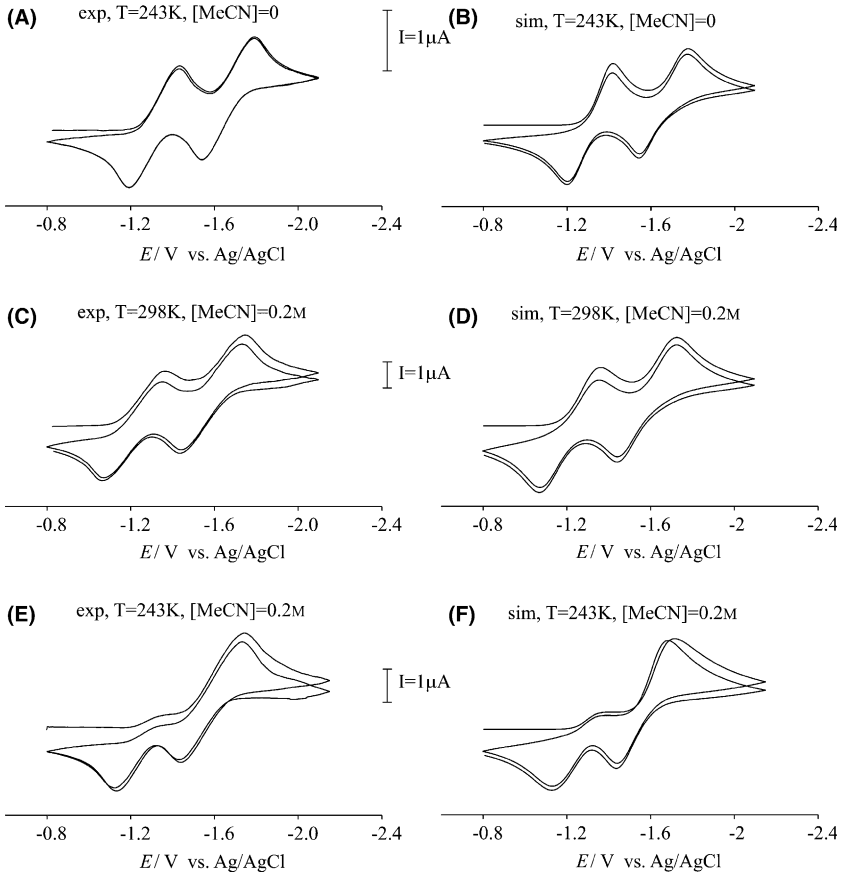

Fig. 3. Experimental (A, C, E) and simulated (B, D, F) cyclic voltammograms of complex *rac*-**10** at different temperatures and acetonitrile concentrations.

Table 3
Half-wave peak potentials $E^1_{1/2}$ and $E^2_{1/2}$ (V) and potential difference $\Delta E = E^1_{1/2} - E^2_{1/2}$ of *rac*-**10**, *meso*-**10** and **II** in thf versus Ag/AgCl at scan rates $v = 100$ mV s^{-1}

	$E^1_{1/2}$ (V)	$E^2_{1/2}$ (V)	ΔE (V)
rac-**10**	−0.95	−1.33	0.380
meso-**10**	−1.25	−1.64	0.390
[Ir(tropp^{Ph})$_2$]Otf (**II**)	−0.97	−1.43	0.460

was characterised by NMR spectroscopy and characteristic ^{1}H and ^{13}C NMR data are listed in Table 4. The non-equivalent ^{31}P resonances indicate that *rac*-**13** has a trigonal bipyramidal structure in which one phosphorus atom (20.1 ppm) occupies an equatorial position, the other one an axial position (27.8 ppm). As observed for the penta-coordinated iridium complexes, *meso*/*rac*-**9** with the bis(tropp^{Ph})ethane ligand, the differences between the chemical shifts of the coordinated C=C units in equatorial and axial position are significant.

For the ^{13}C NMR signals, a large difference is recognised. The axial olefin is shifted by about 85 ppm to lower frequencies when compared to the free ligands *rac*/*meso*-**7** (see data on the bottom of Table 4). The olefin unit in axial position is shifted by only 20 ppm. Hence, while the axial olefin mainly binds via ligand-to-metal donation, the olefin in the equatorial site experiences a significant metal-to-ligand back-donation and concomitantly the metalla cyclopropane character is much more pronounced. Noteworthy is the observation of a strongly shielded resonance for one of the central CH_2 protons (−0.01 ppm) in the propylene bridge, which is again caused by the placement above the magnetic ring current of one of the tropp-benzo groups (see Fig. 5 below for an illustration).

The thermodynamic data for the reaction, *rac*-**10** + MeCN ⇆ *rac*-**13**, were determined by recording the ^{31}P NMR spectra at various temperatures. At 298 K, an equilibrium constant $K = 45.8$ M^{-1} corresponds to a free reaction enthalpy $\Delta G^{298}_r = -9.5$ kJ mol^{-1} ($\Delta H^{298}_r = -48$ kJ mol^{-1}, $\Delta S^{298}_r = -129$ J K^{-1} mol^{-1}).

Fig. 3(A) shows the cyclic voltammogram (CV) obtained with *rac*-**10** in CH_2Cl_2/1 M (nBu$_4$N)$^+$PF$_6^-$ at 243 K. When MeCN is added (0.2 M), the CV at 298 K displayed in Fig. 3(C) is recorded. In Fig. 3(E), the CV under the same conditions but at a lower temperature (243 K) is given. To the right side of each experimental CV, the simulated curves are depicted which were obtained with the DIGISIM 3.02 program

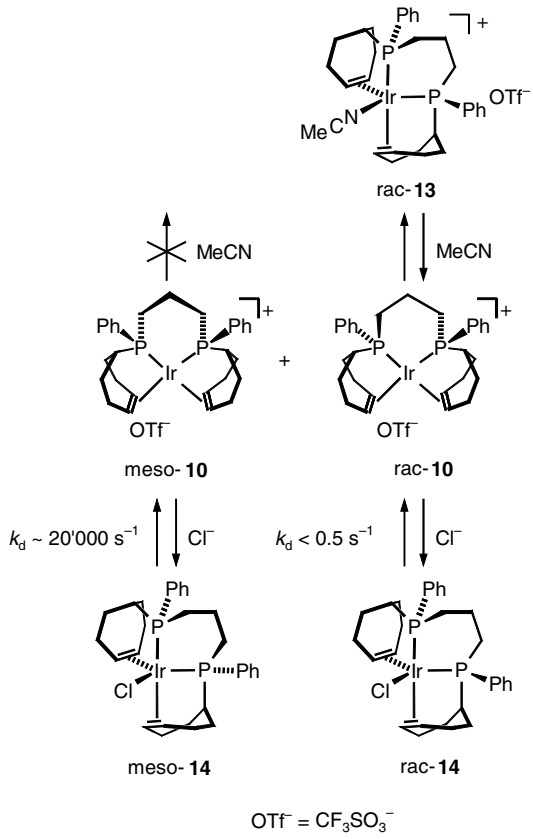

Scheme 6. Reaction of *meso*-**10**, *rac*-**10** with acetonitrile and chloride to give the penta-coordinated iridium(I) complexes *rac*-**13** and *meso*-**14** and *rac*-**14**.

[22,23]. The following mechanism was used for the data simulation

$$[\mathrm{Ir(bis(tropp^{Ph})propane)}]^+ + \mathrm{e}^- \quad (\text{rac-}\mathbf{10}) \rightarrow [\mathrm{Ir(bis(tropp_{Ph})propane)}]^0 \quad (\text{rac-}\mathbf{11}) \qquad (1)$$

$$[\mathrm{Ir(bis(tropp^{Ph})propane)}]^0 + \mathrm{e}^- \quad (\text{rac-}\mathbf{11}) \rightarrow [\mathrm{Ir(bis(tropp^{Ph})propane)}]^- \quad (\text{rac-}\mathbf{12}) \qquad (2)$$

$$[\mathrm{Ir(bis(tropp^{Ph})propane)}]^+ \quad (\text{rac-}\mathbf{10}) + \mathrm{MeCN} \leftrightarrows [\mathrm{Ir(MeCN)(bis(tropp^{Ph})propane)}]^+ \quad (\text{rac-}\mathbf{13}) \qquad (3)$$

$$[\mathrm{Ir(bis(tropp^{Ph})propane)}]^+ \quad (\text{rac-}\mathbf{10}) + [\mathrm{Ir(bis(tropp^{Ph})propane)}]^- \quad (\text{rac-}\mathbf{12}) \rightleftarrows 2\ [\mathrm{Ir(bis(tropp^{Ph})propane)}]^0 \quad (\text{rac-}\mathbf{11}) \qquad (4)$$

Eqs. (1) and (2) represent the charge transfer reactions and Eqs. (3) and (4) the homogeneous chemical reactions in this Scheme. The NMR spectroscopically determined ΔH_r and ΔS_r values were used to calculate the equilibrium constant K for Eq. (3) at various temperatures and these were used in the simulations. The rate constants $k_f^{(3)}$, $k_d^{(3)}$ for the formation and dissociation reaction, respectively, in equilibrium (3) are thus obtained and listed in Table 5.

The agreement between the experimental and simulated curves is satisfactory and ensures that the mechanism (1)–(4) includes all relevant steps. The formation reaction leading to *rac*-**13** in (3) is sufficiently slow and the dissociation sufficiently fast to allow the observation of the *rac*-**10**/*rac*-**11** redox wave in the presence of a 0.2 M concentration of acetonitrile (Fig. 3(B)) and the cyclic voltammogram resembles the one of pure *rac*-**10** (Fig. 3(A)). Only at lower temperatures, the formation of the penta-coordinated iridium cation [Ir(MeCN)(bis(tropp^{Ph})propane)]$^+$ (*rac*-**13**) in the equilibrium (3) is important enough to depress the reduction wave of [Ir(bis(tropp^{Ph})propane)]$^+$ (*rac*-**10**) (Fig. 3(C)). Note that *rac*-**13** as an 18-electron species is not reduced within the applied potential window. Our experimental set-up did not allow determining the kinetic data for the syn/disproportionation (4) with accuracy, however, the fit of the simulated curves was significantly poorer when Eq. (4) was not taken into account. With an equilibrium constant of $K_{syn} = 4 \times 10^6$ for Eq. (4) at $T = 298$ K, [1] upper values for the rate constants of the synproportionation, $k_{syn}^{(4)} < 4 \times 10^4$ M^{-1} s^{-1}, and disproportionation, $k_{disp}^{(4)} < 1 \times 10^2$ M^{-1} s^{-1}, were estimated.

4.3. Reaction with chloride

When LiCl is added to a thf solution of a mixture of the tetra-coordinated complexes *meso*/*rac*-**10**, a slight colour change occurs. In a ^{31}P NMR spectrum, two slightly broadened doublets at 19 ppm and 33 ppm and a very broad signal at 40 ppm are detected. Cooling the mixture to 235 K leads to a sharpening of the first two doublets [21.0, 33.1 ppm, $^2J(P,P) = 18.6$ Hz] and the broad signal at 40 ppm splits into two broadened doublets at 32.2 and 51.6 ppm. The reversible formation and dissociation of the penta-coordinated iridium chloro complexes, *rac*-**14** and *meso*-**14** shown in Scheme 6, is responsible for these observations. Both compounds were not isolated in substance but the less labile complex *rac*-**14** was fully characterised by NMR methods. For *meso*-**14**, the ^{1}H and ^{13}C NMR signals were still very broad even at low temperatures. Relevant data are listed in Table 4. They are very similar to the data obtained for the acetonitrile complex *rac*-**13** and show that *rac*-**14** has likewise a trigonal bipyramidal structure with one

[1] The difference of the first and second redox wave, $\Delta E = E_{1/2}^1 - E_{1/2}^2 = 380$ mV, gives K_{syn} with $\ln K = (nF/RT)\Delta E$; $(nF/RT) = 38.9$ [V^{-1}] ($n = 1$ electron, $T = 298$ K).

Table 4
Selected NMR data of *rac*-**13** and *rac*-**14**

rac-**13**				*rac*-**14**			
δ ^{1}H		δ ^{13}C		δ ^{1}H		δ ^{13}C	
H^{eq}_{bnz}	5.92	C^{eq}_{bnz}	52.6	H^{eq}_{bnz}	6.05	C^{eq}_{bnz}	53.4
H^{ax}_{bnz}	4.25	C^{ax}_{bnz}	50.6	H^{ax}_{bnz}	4.42	C^{ax}_{bnz}	51.2
H^{eq}_{ol}	4.30	C^{eq}_{ol}	35.3	H^{eq}_{ol}	4.32	C^{eq}_{ol}	42.5
H'^{eq}_{ol}	4.32	C'^{eq}_{ol}	46.7	H'^{eq}_{ol}	5.22	C'^{eq}_{ol}	50.8
H^{ax}_{ol}	6.26	C^{ax}_{ol}	102.5	H^{ax}_{ol}	6.62	C^{ax}_{ol}	106.8
H'^{ax}_{ol}	7.29	C'^{ax}_{ol}	108.7	H'^{ax}_{ol}	7.35	C'^{ax}_{ol}	113.9

Selected NMR chemical shifts (ppm) of uncoordinated *rac*/*meso*-**7**: H_{bnz} 4.09 (*rac*), 4.08 (*meso*); H_{ol} 6.92, 6.86 (*rac* + *meso*); C_{bnz} 60.9 (*rac* + *meso*); C_{ol} 130.4, 130.1 (*rac* + *meso*). Note that only the H_{bnz} resonance can be distinguished while the other resonances are not sufficiently resolved and could not be assigned to one of both isomers.

Table 5
Equilibrium constants, K, and rate constants, k_f, k_d for the formation and dissociation of *rac*-**13**

	[MeCN] = 0.2 M, T = 298 K	[MeCN] = 0.2 M, T = 243 K
$K^{(3)}$ M^{-1}	45	4×10^3
$k_f^{(3)}$ M^{-1} s^{-1}	6×10^3	2×10^5
$K_d^{(3)}$ s^{-1}	1×10^2	44

phosphorus atom (21.0 ppm) in the equatorial and one (33.8 ppm) in the axial position. Noteworthy is again the shielded resonance at −0.01 ppm for one of the protons in the central CH_2 group of the propylene bridge. A line shape analysis of the ^{31}P NMR signals of complexes **14** gives k_d(meso) ≈ 20′000 s^{-1} and k_d(rac) < 0.5 s^{-1}, i.e., the reaction for the *meso*-compound is at least five orders of magnitudes faster than for the racemic mixture of the complexes with the chiral *R*,*R*(*S*,*S*)-configured bis(tropp^{Ph})propane ligand.

4.4. Reaction with dihydrogen

Finally, the reaction of the 16-electron tetra-coordinated complexes, *meso*/*rac*-[Ir(bis(tropp^{Ph})propane)]$^+$, *meso*/*rac*-**10**, with dihydrogen was investigated. We begin our discussion with *rac*-**10** which is used in pure form in the reaction with H_2. The deeply coloured CH_2Cl_2 solution of *rac*-**10** becomes pale-yellow when exposed to 1 atmosphere of H_2 at room temperature. At the beginning of the reaction, a singlet at 67.6 ppm of the non-reacted starting material *rac*-**10**, two doublets at 31.6 ppm (P′) and 49.3 ppm (P, $^2J_{P-P}$ = 6.4 Hz) for compound *rac*-**17**, and two doublets at −6.9 ppm (P′) and 39.4 ppm (P, $^2J_{P-P}$ = 6.3 Hz) for compound *rac*-**19** are detected in the ^{31}P NMR (see Scheme 7 for P, P′, H, H′). After longer reaction times under an H_2-atmosphere and vigorous stirring of the reaction mixture, only the latter doublets are observed. Importantly, when the H_2-atmosphere is replaced by an argon or nitrogen atmosphere, *rac*-**19** slowly reconverts via the intermediate *rac*-**17** to the starting material, i.e., the hydrogen addition reactions to *rac*-**10** are fully reversible. The structures of compounds *rac*-**17** and *rac*-**19** (shown in Scheme 7) were determined by NMR spectroscopy. Additionally, a single crystal X-ray diffraction study was performed for *rac*-**19** (vide infra).

In the region between −7.5 and −13 ppm of the ^{1}H NMR spectrum of the mixture containing *rac*-**17** and *rac*-**19**, multiplets for four different hydrides are observed (Fig. 4).

The sharp resonance at −12.2 ppm [$^2J(H,P) \approx {}^2J(H,P') = 17$ Hz] and the doublet of doublets at −11.6 ppm [$^2J(H',P') = 109$ Hz, $^2J(H',P) = 15$ Hz] are assigned to the H and H′ hydrides, respectively, in compound *rac*-**17**. The slightly broadened doublet of doublets at −9.5 ppm [$^2J(H',P') = 122$ Hz, $^2J(H',P) = 13$ Hz] is assigned to the H′ and the broadened signal at −8.0 ppm [$^2J(H,P) \approx {}^2J(H,P') = 13$ Hz] to the H nucleus in trans position to the triflate group in *rac*-**19**.

The ^{31}P NMR signal at −6.9 ppm in *rac*-**19** is characteristic for a phosphorus nucleus of a tropp system where the 5H-dibenzo[*a*,*d*]cycloheptene unit is not bonded to the metal (see also P2 in *meso*/*rac*-**9**). Furthermore, proton resonances at 2.28 and 2.88 ppm are observed which are typical for CH_2 groups in a saturated 10,11-dihydro-5H-dibenzo[*a*,*d*]cycloheptene unit [24]. Two resonances at 4.19 and 5.28 ppm are observed for the olefinic protons of the coordinated trop moiety. In the ^{13}C NMR spectrum, the resonances for the C=C$_{trop}$ are not resolved and only one signal at 74 ppm is observed. When compared to the related iridium(III) hydride, [IrH_2(tropp^{Ph})$_2$]$^+$ **IV** (C=C$_{trop}$ resonances: ^{1}H: 5.31 ppm, ^{13}C 82.7, 83.9 ppm) [25], the chemical shifts in *rac*-**19** indicate a slightly higher back-donation from the iridium centre to the tropp ligand. Note again the observation of a deshielded proton resonance for one of the CH_2 protons in the centre position of the propylene bridge at −0.06 ppm.

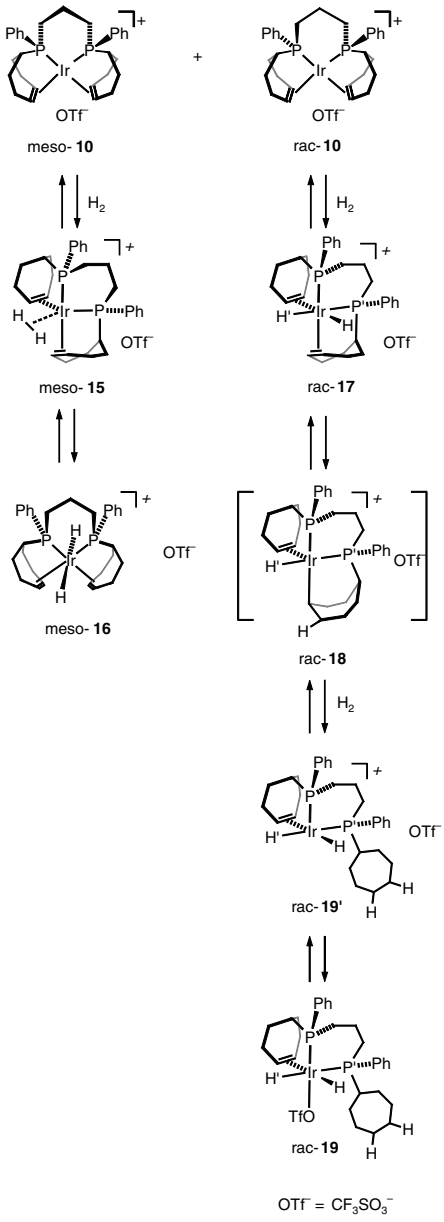

Scheme 7. Synthesis of the iridium(III) dihydride complexes, *meso*-**16** and *rac*-**19**, including proposals for their formations.

The result of the X-ray structure analysis [2] for *rac*-**19** is in full accord with the NMR data. The cation of *rac*-**19** is shown in simplified form in Fig. 5, selected bond lengths and angles are given in the Figure caption. The hydrides at the iridium centre were located in the Difference Fourier Synthesis and refined without constraints.

The two Ir–P distances are quite different [Ir–P1 2.189(1) Å, Ir–P2 2.395(1) Å] and the longer one reflects the well-established strong *trans*-influence of the hydride ligand. The distance between Ir and the centroid of the coordinated carbon–carbon double bond (2.160 Å) as well as the length of that C4═C5 bond (1.423 Å) fall within the usual range. The P1–Ir–P2 bite angle (98.8°) is slightly larger than the ideal 90° angle in an octahedron. Noteworthy is the semi-chair conformation of the central Ir–P1–C22–C23–C24–P2 chelate ring which is emphasised in the bottom of Fig. 5. This places one of the hydrogen atoms at C23 close to the centroid of one of the tropp benzo rings (2.60 Å, see Fig. 5) and indeed explains the unusual low frequency shift of this proton.

Although the Ir–O1 bond to the coordinated triflate anion, $O_3SCF_3^- = OTf^-$, has a usual length [2.205(3) Å], the ^{19}F NMR spectrum shows two broadened resonances at −76.8 and −79.2 ppm which we attribute to the coordinated and un-coordinated OTf^-, respectively. We used the Forsèn-Hofmann magnetisation transfer technique [26] in order to determine the rate for the dissociation process (Fig. 6). With this method, we found a rate $k_d = 29\ s^{-1}$ and hence the dissociation is a rather slow process. We assume that this dissociation to the highly reactive Ir(III) complex *rac*-**19**′ which on electronic grounds should have a square pyramidal structure, is the initial step in the re-formation of the starting complex *rac*-**10** which proceeds by consecutive C–H activation steps and H_2-losses as shown in Scheme 7.

In the first, non-observed intermediate the C35–H bond of the cycloheptane ring will coordinate to the vacant coordination site in *rac*-**19**′ triggering H_2-elimination and oxidative addition of the C35–H bond. Thereby, *rac*-**18** is obtained as a second non-observable intermediate. Subsequent β-hydrogen elimination gives *rac*-**17** which is clearly observed by NMR spectroscopy. Finally, *rac*-**17** looses a second equivalent of H_2 and the starting complex *rac*-**10** is obtained in quantitative yield. Note that it is the first time that we observe the hydrogenation of a coordinated tropp ligand. The reason may be here that the central six-membered ring in *rac*-**18** is strained, which provokes a twist around the Ir–C bond of the trop unit. At this point, the thermodynamically favoured microscopic reverse, i.e., β-H elimination in *rac*-**18** to produce *rac*-**17**, is suppressed because the necessarily parallel arrangement of the Ir–H bond and $C{=}C_{trop}$ unit is removed [27]. Instead, a reductive elimination occurs and a concomitant oxidative addition of a second equivalent H_2 leads to *rac*-**19**. Note also that the insertion reaction in *rac*-**17** is highly selective and occurs exclusively into the coordinated $C{=}C_{trop}$ bond

[2] The structure was solved by direct methods, all atoms except hydrogen were refined anisotropically (SHELXTL ver. 6.12). H1 and H2 (hydrides) were freely refined isotropically, the other hydrogen atoms were treated with a riding model. Empirical absorption correction: SADABS ver. 2.03. $C_{46}H_{42}F_3IrO_3P_2S$; cuboid, crystal size 0.19 × 0.18 × 0.15 mm; monoclinic, space group $P2_1/c$, $a = 15.443(2)$, $b = 12.428(1)$, $c = 23.002(2)$ Å, $\beta = 108.032(2)°$, $V = 4197.6(8)$ Å^3, $Z = 4$, $\mu = 3.36$ mm^{-1}; λ(Mo Kα) = 0.71073 Å, $T = 293$ K, $2\theta_{max}/2\theta_{min} = 54.20°/3.72°$, collected (independent) reflections = 25,222 (9206), $R_{int} = 0.0414$; 513 refined parameters, $R_1 = 0.0356$ for 6648 reflections with $I > 2\sigma$, $wR_2 = 0.0861$ for all data, GooF on $F^2 = 1.002$, max./min. residual electron density = 1.95/−1.22 e/Å^3.

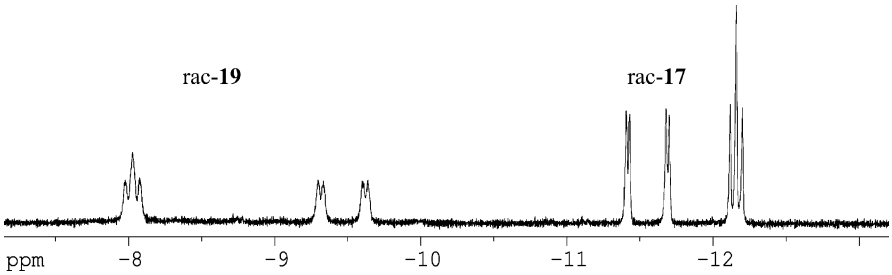

Fig. 4. Section of the ^{1}H NMR spectrum of *rac*-**17** and *rac*-**19** showing the hydride resonances.

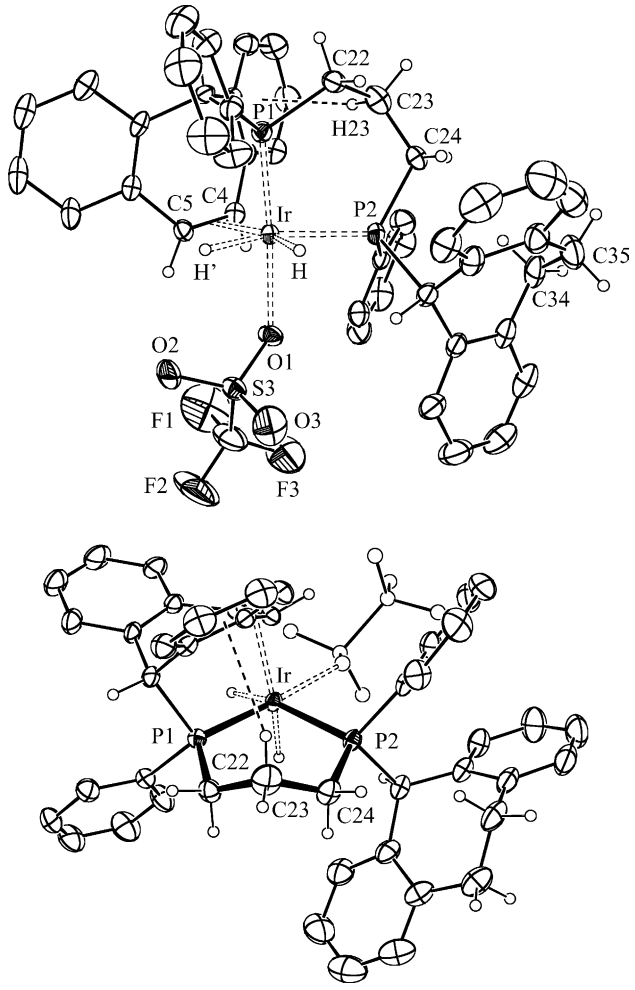

Fig. 5. Structure of the cation of *rac*-**19**. For clarity, the hydrogen atoms at the benzo groups of the 5H-dibenzo[*a*,*d*]cycloheptene moieties and phenyl groups on the phosphorus atoms have been omitted. Top: View from the side of the hydrides; bottom: view on the central six-membered chelate ring demonstrating the semi-chair conformation. The distance between H23 in the propylene bridge to the centre of one benzo group at 2.6 Å is indicated by a thin dotted line. Selected bond lengths [Å] and angles [°]. Ct indicates the centroid of the C4–C5 bond: Ir–P(1) 2.189(1), Ir–P(2) 2.395(1), P(1)–C(22) 1.834(5), C(22)–C(23) 1.519(8), C(23)–C(24) 1.488(7), P(2)–C(24) 1.836(5), Ir(1)–C(4) 2.296(4), Ir(1)–C(5) 2.252(4); Ir(1)–O(1) 2.205(3), C(4)–C(5) 1.423(6); P(1)–Ir(1)–O(1) 176.0(1), P(1)–Ir(1)–Ct 92.0(1), C(5)–Ir(1)–C(4) 36.5(1), P(1)–Ir(1)–P(2) 98.8(1), O(1)–Ir(1)–P(2) 85.2(1), Ct–Ir(1)–P(2) 107.6(1), P(1)–Ir(1)–H(1) 90(2), P(2)–Ir(1)–H(1) 87(2), P(1)–Ir(1)–H(2) 88.4(2), O(1)–Ir(1)–H(2) 88.0(2), Ct–Ir(1)–H(2) 90.1(2), P(2)–Ir(1)–H(2) 160.4(2), H(1)–Ir(1)–H(2) 75(3), H(1)–Ir(1)–Ct 165(3).

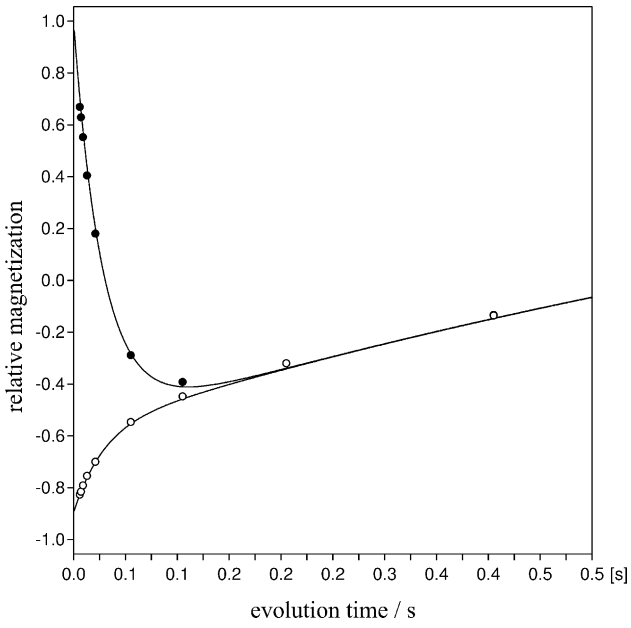

Fig. 6. Plot of the relative magnetisation of the ^{19}F nuclei in the complexed and unbonded triflate anion, $CF_3SO_3^-$, versus the evolution time [s^{-1}] obtained with a solution of *rac*-**19** in CH_2Cl_2 at $T = 273$ K.

that has two hydrogen centres in *cis*-position. The other C═C_{trop} bond in *cis*-position to H′ but *trans*-position to H (see Scheme 7) remains unaffected despite its coplanar arrangement with the Ir–H′ bond which would allow the insertion. This observation underlines the stability of a [IrH_2(C═C)] system versus [IrH(CCH)].

The reaction of the *meso*-isomer of the tetra-coordinated [Ir(bis(tropp^{Ph})propane)]$^+$ cation, *meso*-**10**, with H_2 proceeds differently. When a CH_2Cl_2 solution of *meso*-**10** is kept under an atmosphere of H_2, the intensity of the singlet at 57.7 ppm in the ^{31}P NMR spectrum for *meso*-**10** decreases as the intensity of a new singlet at 51.6 ppm increases. The reaction is faster than the previously discussed reaction with *rac*-**10** and finally only the signal at 51.6 ppm for the product *meso*-**16** is observed (aside small amounts of *rac*-**19** which stem from the 10% *rac*-**10** always present as impurity in *meso*-**10**). The compound *meso*-**16** is labile and when the H_2-atmosphere is replaced by an atmosphere of argon, the starting complex *meso*-**10** is fully recovered by loss of H_2. *meso*-**16** was undoubtedly characterised NMR

spectroscopically as a further example of a *trans*-dihydride which is relatively rare compared to the numerous *cis*-dihydride compounds [28]. In the ^{1}H NMR spectrum each hydride is observed as a doublet of triplets at −9.97 and −8.75 ppm with similiar couplings of $^2J(P,H)$–$^2J(H,H) = 12.5$ Hz, which are typical for *trans*-$^2J(H,H)$ and *cis*-$^2J(P,H)$ coupling constants. The resonances of the two inequivalent olefinic protons of the coordinated C=C$_{trop}$ units are observed at 5.27 and 5.49 ppm while the benzylic protons in the tropp^{Ph} have identical chemical shifts (4.79 ppm) in accord with the C_s-symmetric structure of *meso*-**16** shown in Scheme 7. To explain the formation of the *trans*-dihydride *meso*-**16**, we assume that due to the steric constraints imposed by the ligand system, H_2 cannot be oxidatively added to the iridium centre but binds as H_2-molecule. Coordinated H_2 can be quite acidic and may eventually be deprotonated even by triflate to give traces of HSO_3CF_3 (heterolytic cleavage of H_2). This acid may then rapidly protonate the mono-hydride intermediate [IrH(bis(troppPh)propane)] to give *meso*-**16** as the thermodynamically stable product in this system. Note in this context that all our attempts to synthesise this mono-hydride complex, either by deprotonation of *meso*-**16**, reaction of hydride sources (i.e., $NaBH_4$, $LiBEt_3H$) with *meso*-**10**, or protonation of the anionic complex *meso*-**12** failed.

5. Discussion and conclusions

The reactions of acetonitrile (as archetypical neutral 2-electron donor) and chloride (as archetypical anionic 2-electron donor) with the tetra-coordinated 16-electron complexes *cis*/*trans*-[Ir(tropp^{Ph})$_2$]$^+$ (*cis*/*trans*-**II** in Scheme 1) were previously studied [22] and the following data for the equilibria (5) and (6) were obtained at 298 K

$$\underset{\textit{cis/trans}\text{-}\mathbf{II}}{\textit{cis/trans}\text{-}[\mathrm{Ir}(\mathrm{tropp}^{\mathrm{Ph}})^2]^+} + \mathrm{MeCN} \leftrightarrows \underset{\mathbf{III}\text{-acn}}{[\mathrm{Ir}(\mathrm{MeCN})(\mathrm{bis}(\mathrm{tropp}^{\mathrm{Ph}})\mathrm{propane})]^+}$$

$$K^{(5)} = 626\ \mathrm{M}^{-1}, \quad k_f^{(5)} = 2.6 \times 10^6 \mathrm{M}^{-1}\ \mathrm{s}^{-1}, \quad k_d^{(5)} = 3.7 \times 10^3\ \mathrm{s}^{-1} \qquad (5)$$

$$\underset{\textit{cis/trans}\text{-}\mathbf{II}}{\textit{cis/trans}\text{-}[\mathrm{Ir}(\mathrm{tropp}^{\mathrm{Ph}})_2]^+} + \mathrm{Cl}^- \leftrightarrows \underset{\mathbf{III}\text{-Cl}}{[\mathrm{IrCl}(\mathrm{tropp}^{\mathrm{Ph}})_2]}$$

$$K^{(6)} = 1.7 \times 10^4\ \mathrm{M}^{-1}, \quad k_f^{(6)} = 1.4 \times 10^5\ \mathrm{M}^{-1}\ \mathrm{s}^{-1}, \quad k_d^{(5)} = 8\ \mathrm{s}^{-1} \qquad (6)$$

The complex [Ir(tropp^{Ph})$_2$]$^+$ exists in the form of a *cis*- and a *trans*-isomer (12:88 ratio) and we were unable to determine the equilibrium constant K and rate constants k_f, k_d, separately for both isomers. We assumed, however, that the reactions involving the *cis*-isomers are much slower than for the *trans*-isomers and the data for Eqs. (5) and (6) are actually good estimates for the reactions with the *trans*-isomer. A comparison with the data ($K^{(3)} = 45$ M^{-1}, $k_f^{(3)} = 6 \times 10^3$ M^{-1} s^{-1}, $k_d^{(3)} = 1 \times 10^2$ s^{-1}; vide supra) obtained for the reaction of the C_2-symmetric *R*,*R*(*S*,*S*)-configured complex *rac*-[Ir(bis(tropp^{Ph})propane)]$^+$, *rac*-**10**, evidently a *cis*-isomer, with acetonitrile to give the penta-coordinated [Ir(MeCN)(bis(tropp^{Ph})propane)]$^+$, *rac*-**13**, fully supports this assumption. The formation of *rac*-**13** is three orders of magnitudes slower than the formation of **III**-acn. Further steric hindrance does not allow to detect any reaction with the complex *meso*-**10** containing the other stereoisomer of the tetra-chelating ligand bis(tropp^{Ph})propane, *meso*-**7**, i.e., the formation of k_f may be too small and the dissociation of k_d too fast in order to observe *meso*-**13** on the NMR time scale.

This is seen with the chloro complexes [IrCl(bis(tropp^{Ph})propane)], *meso*-**14** and *rac*-**14**. As in the case of [IrCl(tropp^{Ph})$_2$] (**III**-Cl), they are more stable than the corresponding penta-coordinated acetonitrile complexes and both, *meso*-**14** and *rac*-**14**, are observed by NMR spectroscopy. However, the *meso*-isomer, *meso*-**14**, dissociates at least 40'000 times faster than the C_2-symmetric isomer *rac*-**14**.

The oxidative addition reactions of dihydrogen also demonstrate the reluctance of the tetra-coordinated complex *meso*-**10** to expand its coordination sphere. While *rac*-**10** forms a *cis*-dihydride via homolytic H–H cleavage, with the *meso*-isomer, the H_2 molecule is heterolytically cleaved and an unusual *trans*-dihydride is obtained. Likely, an acidic "non-classical" η^2-bonded H_2 complex is an intermediate. On the other hand, with *rac*-**10** a hydrogenation of a bonded C=C$_{trop}$ unit could be observed for the first time, which indicates that also the *R*,*R*(*S*,*S*)-configured ligand bis(tropp^{Ph})propane imposes some strain energy which provokes a dissocation from the metal centre. This intramolecular hydrogenation is selective and only the C=C$_{trop}$ unit having the two hydride ligands in *cis*-position is hydrogenated.

All these phenomena are caused by the fact that the *R*,*S*-configured ligand *meso*- bis(tropp^{Ph})propane, *meso*-**7**, confines the coordination sphere at the iridium centre to a more planar one impeding geometries necessarily demanding a ligand distortion. More quantitative evidence comes from electrochemical data showing that the 16-electron Ir(I) complex *meso*-**10** with a planar coordination sphere at the metal atom is more difficult to reduce by about 200 mV to the 17-electron Ir(0) complex than the C_2-symmetrical isomer *rac*-**10**. The latter Ir(I) cation has already the tetrahedrally distorted structure which the Ir(0) complex with a d^9 valence electron configuration prefers on electronic grounds. In other words, in the reduction (oxidation) process a strain energy, ΔE_{strain}, of about 20 kJ mol^{-1} is built up (released). If we take ΔE_{strain} as an approximation of the steric contribution to the

activation barriers, which need to be overcome when a further ligand is added either to *rac*-**10** or *meso*-**10**, reactions with *rac*-**10** will be at least 3000 times faster. [3]

The higher stability of the *meso*-isomer of the penta-coordinated complex [Ir(cod)(bis(tropp^{Ph})ethane)]$^+$, *meso*-**9**, in the intra-molecular replacement of one co-ordinated for one non-coordinated C=C$_{trop}$ unit (Scheme 4), which does not change the identity of the complex, cannot be compared with the reactions discussed for the propylene bridged compounds *meso*/*rac*-**10** where the ligand acts as tetra-dentate chelate ligand. These substitutions with the bis(tropp^{Ph})ethane ligand merely serving as a tridentate ligand, likely proceed by dissociation of the only coordinated C=C$_{trop}$ bond to give a tetra-coordinated intermediate. It is reasonable to assume that such a process is more difficult when both bulky tropp groups have to be placed on the same side with respect to the P–Ir–P plane, which is the case in the reaction with *meso*-**9**.

Useful NMR data were obtained in this study which allow to distinguish between equatorially and axially bonded olefins in iridium complexes with coordination number five. It is found that axially placed olefins show relatively small coordination shifts ($\Delta\delta \approx -20$) indicating modest metal-to-ligand back-donation, while the $\Delta\delta$ values for olefins in (the usually encountered) equatorial sites are significant ($\approx$−80 ppm). Finally, we note that in all compounds with an *R*,*R*(*S*,*S*)-configured ligand, *rac*-**6** or *rac*-**7**, and in *meso*-**9** a strongly shielded resonance for one CH_2-proton in the ethylene or propylene bridge is observed. A structure analysis (Fig. 5) for one derivative shows that the placement of one C–H bond over the magnetic ring current of one of the benzo-groups in the ligand is the reason. Obviously, this structural motif highlighted in Figs. 1 and 5 is retained in all these structures which underlines the rigidity of the tropp-ligand system which proved to be helpful in mechanistic investigations.

6. Experimental

6.1. General techniques

All syntheses were performed in flame-dried glassware under an atmosphere of argon using standard Schlenk techniques. Solvents were freshly distilled from sodium (toluene), sodium/benzophenone (THF), from sodium/tetraglyme/benzophenone (hexane) or calcium hydride (dichloromethane) prior to use. Air-sensitive compounds were stored and weighted in an argon filled glove box (Braun MB 150 B-G system) and reactions on small scale were performed directly in the glove box.

[3] This follows from the relation $\ln k_1/k_2 = (\Delta G^{\#2} - \Delta G^{\#1})/RT$.

6.2. NMR

NMR spectra were either taken on Bruker Avance spectrometers operating at 500, 400, 300, or 250 MHz for ^{1}H, respectively. The chemical shifts are given as dimensionless δ values and were referenced against tetramethylsilane (tms) for ^{1}H and ^{13}C, 85% H_3PO_4 for ^{31}P, and $CFCl_3$ for ^{19}F NMR spectra. Coupling constants *J* are given in Hertz [Hz] as absolute values. Whenever the multiplicity of the signals could be analysed, this is discussed in the main body of the text (see Tables 1, 2 and 4) and indicated as s, d, t, q, or m for singlets, doublets, triplets, quartets, or multiplets, respectively. Here, we list only resonances of diagnostic value without further details. The equatorial atom in compounds with a trigonal bipyramidal structure is assigned by as (eq), axial atom as (ax), the atoms of a metal coordinated tropp ligand are indicated as (c) and non-coordinated atom by (nc).

6.3. UV/Vis

The UV/Vis-spectra were measured with the UV–Vis Lambda 19 spectrometer in 0.5-cm quartz cuvettes. Mass spectra were taken on a Finnigan MAT SSQ 7000 in the EI (70 eV) mode.

6.4. X-ray crystallography

Single crystals of *rac*-**6** were obtained by slow diffusion of *n*-hexane into a concentrated CH_2Cl_2 solution. A Bruker AXS APEX (CCD) system was used for the data collection.

6.5. Cyclovoltammetry

The electrochemical investigations were performed on an apparatus designed by Heinze and coworkers [29]. Working electrode: planar platinum electrode (approx. surface area 0.785 mm^2); reference electrode: silver; counter-electrode: platinum wire; tetrahydrofuran as solvent. At the end of each measurement, ferrocene was added as internal standard for calibration (+0.352 V versus Ag/AgCl) and the redox potentials are given versus Ag/AgCl.

6.6. Determination of the equilibrium constant of Eq. (3)

The equilibrium constant at ambient temperature, $K_{298\,K} = 46$ L mol^{-1}, for the reaction, [Ir(bis(tropp^{Ph})propane)]$^+$ (*rac*-**10**) + MeCN ⇆ [Ir(MeCN)(bis(tropp^{Ph})propane)]$^+$ (*rac*-**13**), was extrapolated from the van't Hoff plot obtained with three equilibrium constants at $T = 270.1$, 274.8, and 279.4 K which were determined to 351, 218, and 173 L mol^{-1}, respectively. In the experiment, we used 5.8 mg [Ir(bis(tropp^{Ph})pro-

pane)]Otf (*rac*/*meso*-**10**) as 85:15 mixture of the *meso*:*rac* diastereomers which were dissolved in 0.5 mL CH_2Cl_2 containing 4% (v/v) C_6D_6. The concentration of the *rac*-isomer in this solution was 0.9 μM. The reactant MeCN (100 μL of a 57.0 mM solution in CH_2Cl_2) was added and $^{31}P\{^1H\}$ NMR spectra were recorded with a repetition time of 18.6 s. The peak areas were obtained by Lorentz deconvolution. Exact temperatures were determined with a thermo-coupler fitted in a NMR tube which was introduced into the spectrometer. The van't Hoff plot provided also the enthalpy and entropy of the above written reaction, $\Delta_r H^0 = -48$ kJ mol^{-1}, $\Delta_r S = -129$ J mol^{-1} K^{-1}.

6.7. Syntheses

6.7.1. Synthesis of 1,3-bis[(5H-dibenzo[a,d]cyclohepten-5-yl)phenylphosphino]-propanes R,R/S,S-bis(tropp^{Ph})propane (rac-7) and R,S-bis(tropp^{Ph})propane (meso-7)

A solution of 1 g of 1,3-bis(phenylphosphano)propane **4** [19] (3.8 mmol) in toluene (50 mL) was added to a solution of 1.74 g of 5-chloro-5H-dibenzo[*a*,*d*]cycloheptene **5** (7.6 mmol) in toluene (50 mL) at room temperature leading to the precipitation of the hydrophosphonium salt [(trop)PhHP–$(CH_2)_3$–PH(Ph)(trop)]$^{2+}$ 2Cl$^-$ as a white solid. After stirring for 2 h at room temp., a 1 M solution of potassium carbonate was added and the reaction mixture was stirred for a further 14 h at room temp., and then refluxed until the organic phase became slightly yellow. Subsequently, the organic layer was separated, dried over $CaCO_3$ and the solvent removed under reduced pressure. The residue was re-crystallised from ethanol (30 mL), leading to the formation of a white crystalline precipitate consisting of the diastereomers *rac*-**7** and *meso*-**7** (1.6 g, 66%); m.p. (mixture): 162–166 °C. Elemental *Anal*. Calc. for $C_{45}H_{38}P_2$ (640.75 g mol^{-1}): C, 84.35; H, 5.98. Found: C, 84.53, H, 6.01%. MS (70 eV): *m*/*z* (%): 449.1 (14) [M$^+$ − trop], 258.0 (2) [M$^+$ − 2trop], 191.2 (100) [trop$^+$]. IR (cm^{-1}): $\tilde{\nu}$ 3044 m, 1633 w, 1592 s, 1489 m, 1458 w, 1435 m, 1200 w, 1159 m, 1105 m.946 w, 807 s, 486 s, 765 s, 745 s, 693 s, 711 s, 642 s, 617 m. *rac*-**7**: Only some of the NMR signals of the *rac*-**7**/*meso*-**7** mixture were sufficiently resolved and could be assigned either to the *rac*- or *meso*-isomer; diagnostic NMR parameters are listed here: ^{1}H NMR (500.2 MHz, $CDCl_3$): $\delta = 0.97$ [1H, PCH_2CHHCH_2P(*meso*)], 1.23 [2m, 3H, PCH_2–CH_2–CH_2P(*meso* + *rac*)], 1.40 [2m, 4H, $PCHH$–CH_2–$CHHP$(*meso* + *rac*)], 1.80 [m, 2H, PCHH–CH_2–CHHP(*meso*)], 1.89 [m, 2H, PCHH–CH_2–CHHP(*rac*)], 4.08 [d, 2H, $^2J_{P,H} = 5.7$ Hz, CHP(*meso*)], 4.09 [d, 2H, $^2J_{P,H} = 5.7$ Hz, CHP(*rac*)], 6.86 (2d, 4H, =C*H*), 6.92 (2d, 4H, =C*H*). ^{13}C NMR (125.7 MHz, C_6D_6): $\delta = 23.5$ (2t, $^1J_{P,C} = 19.6$ Hz, $^1J_{P,C} = 18.8$ Hz, 2C, PCH_2–*C*H_2–CH_2P), 29.3–28.9 (4d, $^1J_{P,C} = 19.4$ Hz, 4C, P*C*H_2), 60.8 (2d, $^1J_{PC} = 19.4$ Hz, 2C, *C*HP), 130.1 (2 d, $J_{P,C} = 1.4$ Hz, 2C, = *C*H), 130.4 (2d, $J_{P,C} = 1.4$ Hz, 2C, =*C*H). ^{31}P-NMR (162.0, $CDCl_3$): $\delta = -22.6$(s, 2P, *rac*), −22.8 (s, 2P, *meso*).

6.7.2. Synthesis of the penta-coordinated complexes [Ir{R,S-bis(tropp^{Ph})ethane}(cod)]O_3SCF_3 (meso-9) and [Ir{R,R/S,Sbis(tropp^{Ph})ethane}(cod)]O_3SCF_3 (rac-9) [18]

A solution of 50 mg bis(tropp^{Ph})ethane *meso*/*rac*-**6** [18] (0.08 mmol) in dichloromethane (5 mL) was reacted with a solution of 44 mg [Ir(cod)$_2$]OTf **8** (0.08 mmol) in dichloromethane (5 mL). After stirring for 20 min, the solution mixture was concentrated to 20% of its volume and hexane was added to precipitate the complex, as a microcrystalline deep-red powder (57 mg, 66%): UV–Vis of the mixture of *meso*/*rac*-**9** (CH_2Cl_2): λ_{max}/nm 294, 220. *[Ir{R,S-bis(tropp^{Ph})ethane}(cod)]O_3SCF_3* (*meso*-**9**): m.p. >250 °C. Diagnostic NMR parameters: ^{1}H NMR (500.2 MHz, CD_2Cl_2, 225 K): $\delta = -0.26$ (1H, P_{ax}–CH_2CHH–P_{eq}), 3.68 (1H, =CH_{eq}), 4.59 (1H, C*H*P), 5.51 (1H, =CH_{eq}). ^{31}P NMR (202.5 MHz, CD_2Cl_2, 225 K): $\delta = 12.7$ (s), 66.6 (s). *[Ir{R,R/S,Sbis(tropp^{Ph})ethane}(cod)]O_3SCF_3* (*rac*-**9**): m.p. >250 °C. Diagnostic NMR parameters: ^{1}H NMR (500.2 MHz, CD_2Cl_2, 225 K): $\delta = -0.69$ (1H, P_{ax}–CH_2CH^3H–P_{eq}), 0.60 (1H, P_{ax}–CH^2HCH_2–P_{eq}), 1.69 (1H, P_{ax}–CH^1HCH_2–P_{eq}), 2.45 (1H, P_{ax}–CH_2CH^4H–P_{eq}), 2.53 (1H, =CH_{cod}), 2.88 (1H, =CH_{cod}), 3.94 (1H, =CH_{eq}), 4.05 (1H, =CH_{cod}), 4.92 (1H, CHP_{ax}), 5.60 (1H, =CH_{eq}), 5.84 (1H, CHP_{eq}), 6.64 (1H, =CH_{cod}), 6.64 [1H; =C*H* (nc)], 6.85 [1H, =C*H* (nc)]. ^{13}C NMR (125.8 MHz, CD_2Cl_2, 225 K): $\delta = 25.9$ (1C, $P_{ax}CH_2CH_2P_{eq}$), 27.8 (1C, $PCH_2CH_2P_{eq}$), 49.6 (1C, *C*HP_{ax}), 56.5 (1C, =*C*H_{cod}), 59.5 (1C, =*C*H_{eq}), 59.8 (1C, *C*HP_{eq}), 60.1 (1C, =*C*H_{cod}), 62.3 (1C, =*C*H_{eq}), 92.7 (1C, = *C*H_{cod}), 98.3 (1C, =*C*H_{cod}), 129.3 [1C, =*C*H (nc)], 132.3 [1C, =*C*H (nc)]. ^{31}P NMR (202.5 MHz, CD_2Cl_2, 225 K): $\delta = 39.1$ (1P, P_{eq}), 77.6 (1P, P_{ax}).

6.7.3. Synthesis of the tetracoordinated iridium(I) complexes meso-[Ir{R,S-bis(tropp^{Ph})propane}]O_3SCF_3 (meso-10) and [Ir{R,R/S,S-bis(tropp^{Ph})propane}]O_3SCF_3 (rac-10)

A solution of 100 mg *meso*/*rac*-bis(tropp^{Ph})propane *meso*/*rac*-**7** (0.18 mmol) in CH_2Cl_2 (5 mL) was reacted with a solution of 115 mg [Ir(cod)$_2$]OTf **8** (0.18 mmol) in CH_2Cl_2 (5 mL). After stirring for 20 min, the solution mixture was concentrated to 20% of its volume and hexane was added to precipitate the mixture of the product complexes, *meso*/*rac*-**10**, as a deep microcrystalline powder (145 mg, 82%, *meso*-**10**:*rac*-**10** = 50:50). The diastereomers could be separated by fractional crystallisation in THF. From THF, the *R*,*R*/*S*,*S*-configured compound *rac*-**10** crystallised first in spectroscopically pure form and the *R*,*S*-configured compound

meso-**10** crystallised after addition of hexane in about 90% purity. UV–Vis of the mixture of *meso*/*rac*-**10** (CH_2Cl_2): λ_{max}/nm 452.3, 366.9, 219.5. *[Ir{R,S-bis(tropp^{Ph})propane}]O_3SCF_3* (*meso*-**10**): m.p. >250 °C. Elemental *Anal*. Calc. for $C_{46}H_{38}P_2F_3IrO_3S$ (982.01 g mol^{-1}): C, 56.26; H, 3.90. Found: C, 56.71; H, 4.03%. Diagnostic NMR parameters: ^{1}H NMR (250.1 MHz, CD_2Cl_2): $\delta = 0.90$ (2H, PC*H*$_2$CH$_2$C*H*$_2$P), 2.21 (1H, PCH$_2$C*H*$_2$CH$_2$P), 2.35 (1H, PCH$_2$C*H*$_2$CH$_2$P), 2.75 (2H, PC *H*$_2$CH$_2$C*H*$_2$P), 5.04 (2H, C*H*P), 5.74 (2H, =C*H*), 6.02 (2H, =C*H*). ^{13}C NMR (62.9 MHz, CD_2Cl_2): $\delta = 20.5$ (2C, PC*H*$_2$CH$_2$C*H*$_2$P), 21.2 (1C, PCH$_2$CH$_2$CH$_2$P), 52.1 (2C, *C*HP), 85.0 (2C, =*C*H), 91.8 (2C, =*C*H). ^{31}P NMR (101.3 MHz, CD_2Cl_2): $\delta = 57.7$. *[Ir{R,R/S,S-bis(tropp^{Ph})propane}]O_3SCF_3* (*rac*-**10**): m.p. >250 °C. Diagnostic NMR parameters: ^{1}H NMR (250.1 MHz, CD_2Cl_2): $\delta = 0.97$ (2H, PC*H*$_2$CH$_2$C*H*$_2$P), 1.83 (2H, PCH$_2$C*H*$_2$CH$_2$P), 2.96 (2H, PC*H*$_2$CH$_2$C*H*$_2$P), 5.56 (2H, C*H*P), 5.27 (2H, =C*H*), 6.65 (2H, =C*H*). ^{13}C NMR (62.9 MHz, CD_2Cl_2): $\delta = 16.4$ (1C, PCH$_2$*C*H$_2$CH$_2$P), 18.2 (2C, P*C*H$_2$CH$_2$*C*H$_2$P), 51.6 (2C, *C*HP), 79.7 (2C, =*C*H), 93.2 (2C, =*C*H). ^{31}P NMR (101.3 MHz, CD_2Cl_2): $\delta = 67.6$. UV–Vis (CH_2Cl_2): λ_{max}/nm 469, 364.5.

6.7.4. Synthesis of the iridate complex *[Na(thf)$_6$]$^+$ [Ir{R,R/S,S-bis(tropp^{Ph})propane}]$^-$ (rac-**12**)*

To a suspension of 100 mg of the complex [Ir{*R*,*R*/*S*,*S*-bis(tropp^{Ph})propane}]O_3SCF_3 *rac*-**10** (0.1 mmol) in thf (3 mL), a freshly prepared solution of sodium/naphthalide in thf was added (4.4 mL of a 0.055 M solution = 0.24 mmol). Subsequently, the deep red reaction mixture was filtered to remove NaO_3SCF_3. The solvents were evaporated under reduced pressure and a deep red powder was obtained, which was washed several times with hexane (95 mg, 73%). Diagnostic NMR parameters: ^{1}H NMR (300.1 MHz, [D$_8$]thf): $\delta = 0.84$ (PCH$_2$C*H*$_2$CH$_2$P, 2H), 1.17 (PC*H*$_2$CH$_2$C*H*$_2$P, 2H), 2.09 (PC*H*$_2$CH$_2$C*H*$_2$P, 2H), 2.36 (2H, =C*H*), 3.98 (2H, =C*H*), 4.40 (2 H, C*H*P). ^{13}C NMR (100.6 MHz, [D$_8$]thf): $\delta = 19.6$ (1C, PC*H*$_2$CH$_2$CH$_2$P), 21.2 (1C PCH$_2$CH$_2$CH$_2$P), 21.6 (1C, PCH$_2$CH$_2$CH$_2$P), 22.6 (2C, =*C*H), 37.6 (2C, =*C*H), 52.5 (2C, *C*HP). ^{31}P NMR (121.5 MHz, [D$_8$]thf): $\delta = 74.0$.

6.7.5. Synthesis of the acetonitrile complex *[Ir(MeCN)-{R,R/S,S-bis(tropp^{Ph})propane}]O_3SCF_3 (rac-**13**)*

To a solution of 50 mg of a mixture of [Ir{*R*,*S*-bis(tropp^{Ph})propane}]OTf *meso*-**10** and [Ir{*R*,*R*/*S*,*S*-bis(tropp^{Ph})propane}]OTf *rac*-**10** (0.05 mmol) in 5 mL of THF was added 100 μL of acetonitrile. Both product complexes, *meso*-**13** and *rac*-**13**, could not be isolated but *rac*-**13** was characterised in solution by NMR spectroscopy. Diagnostic NMR parameters: ^{1}H NMR (400.1 Hz, CD_2Cl_2, 225 K): $\delta = -0.38$ (1H, PCH$_2$C*H*$_2$CH$_2$P), 0.52 (1H, P$_{ax}$C*H*$_2$CH$_2$CH$_2$P), 1.24 (1H, PCH$_2$CH$_2$C*H*$_2$P$_{eq}$), 1.80 (1H, PCH$_2$C*H*$_2$CH$_2$P), 2.02 (1H, PCH$_2$CH$_2$C*H*$_2$P$_{eq}$), 2.31 (1H, P$_{ax}$C*H*$_2$CH$_2$-CH$_2$P), 4.25 (1H, C*H*P$_{ax}$), 4.30 (1H, =C*H*$_{eq}$), 4.32 (1H, =C*H*$_{eq}$), 5.92 (1H, C*H*P$_{eq}$), 6.26 (1H, =C*H*$_{ax}$), 7.29 (1H, =C*H*$_{ax}$). ^{13}C NMR (75.5 MHz, CD_2Cl_2, 225 K): $\delta = 18.1$ (1C, P$_{ax}$*C*H$_2$CH$_2$CH$_2$P), 20.0 (1C, PCH$_2$CH$_2$-CH$_2$P), 28.7 (1C, PCH$_2$CH$_2$*C*H$_2$P$_{eq}$), 35.3 (1C, =*C*H$_{eq}$), 46.7 (1C, =*C*H$_{eq}$), 50.6 (1C, *C*HP$_{ax}$), 52.6 (1C, *C*HP$_{eq}$), 102.5 (1C, =*C*H$_{ax}$), 108.7 (1C, =*C*H$_{ax}$). ^{31}P NMR (161.9 MHz, CD_2Cl_2, 225 K): $\delta = 20.2$ [d, ^2J(P, P) = 22.4 Hz, P_{eq}], 26.8 (d, P_{ax}). UV–Vis (THF): λ_{max}/nm: 370, 278.

6.7.6. Synthesis of the chloro complexes *[IrCl{R,S-bis(tropp^{Ph})propane}] (meso-**14**) and [IrCl{R,R/S,S-bis(tropp^{Ph})propane}] (rac-**14**)*

To a solution of 100 mg of a mixture of [Ir{*R*,*S*-bis(tropp^{Ph})propane}]OTf *meso*-**10** and [Ir{*R*,*R*/*S*,*S*-bis(tropp^{Ph})propane}]OTf *rac*-**10** (0.10 mmol) in 5 mL of THF, 4 mg LiCl (0.13 mmol) was added. After stirring for 10 min the reaction was complete (NMR control). Both product complexes, *meso*-**14** and *rac*-**14**, were not isolated. Compound *rac*-**14** was characterised in solution by NMR spectroscopy. *[IrCl{R,S-bis(tropp^{Ph})propane}]* (*meso*-**14**): ^{31}P NMR (161.9 MHz, [D$_8$]THF, 235 K): $\delta = 32.2$ (br), 51.6 (br). *[IrCl{R,R/S,S-bis(tropp^{Ph})propane}]* (*rac*-**14**): Diagnostic NMR parameters: ^{1}H NMR (400.1 MHz, [D$_8$]THF, 235 K): $\delta = -0.01$ (1H, PCH$_2$C*H*$_2$CH$_2$P), 0.70 (1H, P$_{ax}$C*H*$_2$CH$_2$CH$_2$P), 1.21 (1H; PCH$_2$-CH$_2$C*H*$_2$P$_{eq}$), 1.61 (1H, PCH$_2$C*H*$_2$CH$_2$P), 2.06 (1H, PCH$_2$CH$_2$C*H*$_2$P$_{eq}$), 2.49 (1H; P$_{ax}$C*H*$_2$CH$_2$CH$_2$P), 4.32 (1H, =C*H*$_{eq}$), 4.42 (1H, C*H*P$_{ax}$), 5.22 (1H, =C*H*$_{eq}$), 6.05 (1H, C*H*P$_{eq}$), 6.41 (1H, =C*H*$_{ax}$), 7.35 (1H, =C*H*$_{ax}$). ^{13}C NMR (75.5 MHz, [D$_8$]THF, 235 K): $\delta = 18.3$ (1C, P$_{ax}$*C*H$_2$CH$_2$CH$_2$P), 20.4 (1C, PCH$_2$ $_C$H$_2$CH$_2$P), 29.7 (1C, PCH$_2$CH$_2$*C*H$_2$P$_{eq}$), 42.5 (1C, =*C*H$_{eq}$), 51.2 (1C, *C*HP$_{ax}$), 50.8 (1C, =*C*H$_{eq}$), 53.4 (1C, *C*HP$_{eq}$), 106.8 (1C, =*C*H$_{ax}$), 113.9 (1C, =*C*H$_{ax}$). ^{31}P NMR (161.9 MHz, [D$_8$]THF, 235 K): $\delta = 21.0$ [d, ^2J(P, P) = 18.6 Hz, P_{eq}], 33.1 (d, P_{ax}). UV–Vis (THF): λ_{max}/nm: 375, 274.

6.7.7. Synthesis of the trans-dihydride *[Ir(H)$_2${R,S-bis(tropp^{Ph})propane}]O_3SCF_3 (meso-**16**)*

A solution of 30 mg of [Ir{*R*,*S*-bis(tropp^{Ph})propane}]O_3SCF_3 *meso*-**10** (0.03 mmol, contaminated with about 10% *rac*-**10**) in CH_2Cl_2 (0.5 mL) was placed under an atmosphere of H_2. The mixture was vigorously stirred until the solution became colourless. The product *meso*-**16** could not be isolated and was characterised in solution by NMR spectroscopy. Diagnostic NMR parameters: ^{1}H NMR (500.2 MHz, CD_2Cl_2): $\delta = -9.97$ (^2J(P, H)–^2J(H, H) = 12.5 Hz, 1H, Ir-*H*), −8.75 (^2J(P, H)–^2J(H, H) = 12.5 Hz, 1H, Ir–*H*), 1.30 (2H, PC*H*$_2$CH$_2$C*H*$_2$P), 1.77 (1H, PCH$_2$C*H*$_2$CH$_2$P), 2.45 (1H, PCH$_2$C*H*$_2$CH$_2$P), 3.33 (2H, PC*H*$_2$CH$_2$C*H*$_2$P), 4.79 (2H,

C*H*P), 5.27 (2H, =C*H*), 5.49 (2H, =C*H*). ^{13}C NMR (125.8 MHz, CD_2Cl_2): δ = 20.4 (1C; $PCH_2CH_2CH_2P$), 25.1 (C, $PCH_2CH_2CH_2P$), 52.8 (2C, *C*HP), 71.5 (2C, =*C*H), 77.8 (2C, =*C*H). ^{31}P NMR (202.5 MHz, CD_2Cl_2): $\delta = 66.7$.

*6.7.8. Synthesis of the cis-dihydride R,R(S,S)-{Ir(H)$_2$(OTf)[(tropp^{Ph})(H$_2$tropp^{Ph})propane]} (rac-**19**)*

A solution of 30 mg of [Ir{*R*,*R*/*S*,*S*-bis(tropp^{Ph})propane}]$^+$ *rac*-**10** (0.03 mmol) in CH_2Cl_2 (0.5 mL) was placed under an atmosphere of H_2. The mixture was vigorously stirred until the solution became colourless. Subsequently, a colourless crystalline product was precipitated upon addition of 0.5 mL of hexane. In solid form, the product *rac*-**19** is stable for a short while on air but must be kept under an atmosphere of H_2 when stored for longer periods of time. Otherwise, *rac*-**19** looses H_2 and the starting material *rac*-**10** is recovered after some time. A melting point cannot be given and the product was characterised by NMR spectroscopy. Diagnostic NMR parameters: ^{1}H NMR (500.2 MHz, CD_2Cl_2): $\delta = -9.46$ (1H, Ir–*H*′), −8.01 (1H, Ir–*H*), −0.06 (1H, $PCH_2CH_2CH_2P$), 1.03 (1H; $PCH_2CH_2CH_2P$), 1.38 (1H, $PCH_2CH_2CH_2P$), 1.61 (1H, $PCH_2CH_2CH_2P$), 2.30 (1H, $PCH_2CH_2CH_2P$), 2.28 (2H, C*H*$_2$), 2.54 (1H; $PCH_2CH_2CH_2P$), 2.88 (2H, C*H*$_2$), 4.19 (2H; =C*H*), 4.69 [1H, C*H*P (c)], 5.28 (2H, =C*H*), 5.99 [1H, C*H*P (nc)]. ^{13}C NMR (125.8 MHz, CD_2Cl_2): $\delta = 19.2$ (1C, $PCH_2CH_2CH_2P$), 24.3 (1C, $PCH_2CH_2CH_2P$), 28.3 (1C, $PCH_2CH_2CH_2P$), 32.9 (1C, *C*H$_2$), 33.5 (1C, *C*H$_2$), 53.9 (1C, *C*HP), 55.0 (1C, *C*HP), 73.9 (2C, =*C*H). ^{19}F NMR (376.5 MHz, CD_2Cl_2): $\delta = -76.8$. ^{31}P NMR (202.5 MHz, CD_2Cl_2): $\delta = -6.9$ [d, $^2J(P,P) = 6.3$ Hz, *P*′], 39.4 (d, *P*).

Acknowledgements

This work was supported by the Swiss National Science Foundation.

References

[1] In classical experiments, it was demonstrated that narrow angles at the metal centre in four-membered heterocycles like metalladiphosphetanes, [M(η^2-$R_2PCH_2PR_2$)], activate the metal for oxidative additions; see textbooks on organometallic chemistry for relevant examples. A recent work on this topic was published by: H. Urtel, C. Meier, F. Eisenträger, F. Rominger, J.P. Joschek, P. Hofmann, Angew. Chem. Int. Ed. Engl. 40 (2001) 781, and literature cited therein.

[2] (a) M.R. Churchill, S.A. Bezman, Inorg. Chem. 12 (1973) 260;
(b) M.R. Churchill, S.A. Bezman, Inorg. Chem. 12 (1973) 531.

[3] (a) C.P. Casey, G.T. Whiteker, Isr. J. Chem. 30 (1990) 299;
(b) C.P. Casey, G.T. Whiteker, M.G. Melville, L.M. Petrovich, J.A. Gavney, D.R. Powell, J. Am. Chem. Soc. 114 (1992) 5535;
(c) C.P. Casey, L.M. Petrovich, J. Am. Chem. Soc. 117 (1995) 6007.

[4] D.L. Thorn, R. Hoffman, J. Am. Chem. Soc. 100 (1978) 2079.

[5] (a) Review: P.C.J. Kamer, P.W.N.M. van Leeuwen, J.N.H. Reek, Acc. Chem. Res. 34 (2001) 895;
(b) Review: P. Dierkes, P.W.N.M. van Leeuwen, J. Chem. Soc., Dalton Trans. (1999) 1519;
(c) Hydroformylations: L.A. van der Veen, P.K. Keeven, P.C.J. Kamer, P.W.N.M. van Leeuwen, J. Chem. Soc., Dalton Trans. (2000) 2105;
(d) Non-classical hydrides: M. Kranenburg, P.J.C. Kamer, P.W.N.M. van Leeuwen, B. Chaudret, Chem. Commun. (1997) 373;
(e) Cross-couplings: M. Kranenburg, P.J.C. Kamer, P.W.N.M. van Leeuwen, Chem. Commun. (1997) 155.

[6] H.H. Brintzinger, D. Fischer, R. Mülhaupt, B. Rieger, R.M. Waymouth, Angew. Chem. Int. Ed. Engl. 34 (1995) 1143.

[7] D. Churchill, J.H. Shin, T. Hascall, J.M. Hahn, B.M. Bridgewater, G. Parkin, Organometallics 18 (1999) 2403.

[8] (a) Review: I. Manners, Chem. Commun. (1999) 857;
(b) Calorimetry: A. Berebaum, F. Jäckle, A.J. Lough, I. Manners, Organometallics 21 (2002) 2359;
(c) R. Resendes, J.M. Nelson, A. Fischer, F. Jäckle, A. Bartole, A.J. Lough, I. Manners, J. Am. Chem. Soc. 123 (2001) 2116.

[9] J. Thomaier, S. Boulmaâz, H. Schönberg, H. Rüegger, A. Currao, H. Grützmacher, H. Hillebrecht, H. Pritzkow, New J. Chem. 21 (1998) 947.

[10] H. Schönberg, S. Boulmaâz, M. Wörle, L. Liesum, A. Schweiger, H. Grützmacher, Angew. Chem. 109 (1998) 1492.

[11] H. Schönberg, S. Boulmaâz, M. Wörle, L. Liesum, A. Schweiger, H. Grützmacher, Angew. Chem. Int. Ed. Engl. 37 (1998) 1423.

[12] H. Grützmacher, H. Schönberg, S. Boulmaâz, M. Mlakar, S. Deblon, S. Loss, M. Wörle, Chem. Commun. (1998) 2623.

[13] (a) Rh(0): B. Longato, R. Coppo, G. Pilloni, R. Corvaja, A. Toffoletti, G. Bandoli, J. Organomet. Chem. 637–639 (2001) 710;
(b) N. Mézailles, P. Rosa, F. Mathey, P. Le Floch, Organometallics 19 (2000) 2941.

[14] Ir(0): B. Longato, L. Riello, G. Bandoli, G. Pilloni, Inorg. Chem. 38 (1999) 2818.

[15] (a) C.O. Dietrich-Buchecker, J. Guilhem, J.-M. Kern, C. Pascard, J.-P. Sauvage, Inorg. Chem. 33 (1994) 3498, and literature cited therein;
(b) C. Dietrich-Buchecker, J.-P. Sauvage, J.-M. Kern, J. Am. Chem. Soc. 111 (1989) 7791.

[16] (a) S. Kapp, T.P. Keenan, X. Zhang, R. Fikar, J.A. Potenza, H.J. Schugar, J. Am. Chem. Soc. 112 (1990) 3452, and literature cited therein;
(b) W. Kaim, J. Rall, Angew. Chem. 108 (1996) 47;
(c) Angew. Chem. Int. Ed. Engl. 35 (1996) 43.

[17] S. Deblon, H. Rüegger, H. Schönberg, S. Loss, V. Gramlich, H. Grützmacher, New J. Chem. 23 (2001) 83.

[18] C. Laporte, C. Böhler, H. Schönberg, H. Grützmacher, J. Organomet. Chem. 641 (2002) 227.

[19] J. Dogan, J.B. Schulte, G.F. Swiegers, S.B. Wild, J. Org. Chem. 65 (2000) 951.

[20] To our knowledge, there are no comparable complexes described in the literature for which NMR data have been reported. A low frequency shift is usually related to efficient back-bonding: B.E. Mann, B.E. Taylor, ^{13}C NMR Data for Organometallic Compounds, Academic Press, London, 1981, p. 16.

[21] C. Laporte, F. Breher, J. Geier, J. Harmer, A. Schweiger, H. Grützmacher, Angew. Chem. 116 (2004), in press.

[22] F. Breher, H. Rüegger, M. Mlakar, M. Rudolph, S. Deblon, H. Schönberg, S. Boulmaâz, J. Thomaier, H. Grützmacher, Chem. Eur. J., 2003, in press.
[23] M. Rudolph, S.W. Feldberg, DIGISIM 3.0 Software 2001, Bioanalytical Systems Inc., West Lafayette, IN 47906.
[24] S. Deblon, L. Liesum, J. Harmer, H. Schönberg, A. Schweiger, H. Grützmacher, Chem. Eur. J. 8 (2002) 601.
[25] C. Böhler, N. Avarvari, H. Schönberg, M. Wörle, H. Rüegger, H. Grützmacher, Helv. Chim. Acta 84 (2001) 3127.
[26] (a) S. Forsén, R.A. Hoffman, J. Chem. Phys. 39 (1963) 2892;
(b) R.A. Hoffman, S. Forsén, Prog. NMR Spectrosc. 1 (1966) 15.
[27] M.T. Benson, T.R. Cundari, Inorg. Chim. Acta 259 (1997) 91.
[28] (a) B. Rybtchinski, Y. Ben-David, D. Milstein, Organometallics 16 (1997) 3786;
(b) G. Jia, C.P. Lau, J. Organomet. Chem. 656 (1998) 37;
(c) K. Abdur-Rashid, S.E. Clapham, A. Hadzovic, J.N. Harvey, A.J. Lough, K.H. Morris, J. Am. Chem. Soc. 124 (2002) 15104;
(d) A. Immirzi, A. Musco, G. Carturan, U. Belluco, Inorg. Chim. Acta 12 (1975) L23;
(e) R.S. Paonessa, W.C. Trogler, J. Am. Chem. Soc. 104 (1982) 1138;
(f) C.E. Johnson, R. Eisenberg, J. Am. Chem. Soc. 107 (1985) 3148;
(g) P.P. Deutsch, R. Eisenberg, Chem. Rev. 88 (1988) 1147;
(h) D.K. Packett, W.C. Trogler, Inorg. Chem. 27 (1988) 1768;
(i) S. Li, M.B. Hall, Organometallics 18 (1999) 5682.
[29] K. Hinkelmann, J. Heinze, H.T. Schacht, J.S. Field, H. Vahrenkamp, J. Am. Chem Soc. 111 (1989) 5078.